White Rose Research Online

eprints@whiterose.ac.uk
https://eprints.whiterose.ac.uk
Universities of Leeds, Sheffield and York

Deposited via The University of York.

White Rose Research Online URL for this paper:
https://eprints.whiterose.ac.uk/id/eprint/246331/

Version: Published Version

Article:
Özsan, Çağrı, Welsh, Athi, Zineddu, Stefano et al. (2026) Unlocking Iridium Chemical Space for Antibiotic Discovery through One-Pot Combinatorial Synthesis in a Direct-to-Biology Approach. JACS Au. ISSN: 2691-3704

https://doi.org/10.1021/jacsau.6c00813

Reuse
This article is distributed under the terms of the Creative Commons Attribution-NonCommercial-NoDerivs (CC BY-NC-ND) licence. This licence only allows you to download this work and share it with others as long as you credit the authors, but you can't change the article in any way or use it commercially. More information and the full terms of the licence here: https://creativecommons.org/licenses/

Takedown
If you consider content in White Rose Research Online to be in breach of UK law, please notify us by emailing eprints@whiterose.ac.uk including the URL of the record and the reason for the withdrawal request.

UNIVERSITY OF LEEDS
University of Sheffield
UNIVERSITY of York

JACS Au
AN OPEN ACCESS JOURNAL OF THE AMERICAN CHEMICAL SOCIETY

Open Access
This article is licensed under CC-BY-NC-ND 4.0

pubs.acs.org/jacsau
Article

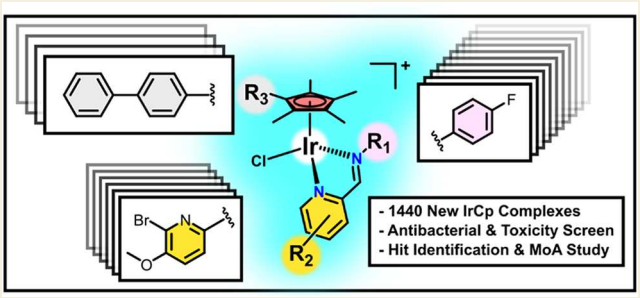
Unlocking Iridium Chemical Space for Antibiotic Discovery through One-Pot Combinatorial Synthesis in a Direct-to-Biology Approach

Çağrı Özsan, Athi Welsh, Stefano Zineddu, David R. Husbands, Kiera Robinson, Anson Kwok-Hei Chau, and Angelo Frei*

Cite This: https://doi.org/10.1021/jacsau.6c00813
Read Online

ACCESS | Metrics & More | Article Recommendations | Supporting Information

ABSTRACT: Antibacterial resistance continues to drive the need for exploring novel chemical spaces beyond conventional organic scaffolds. Metal-based compounds have emerged as a promising class of antibiotic candidates, demonstrating high hit rates against priority bacterial pathogens without exhibiting increased toxicity compared to purely organic molecules. Here, we report a one-pot, three-component combinatorial strategy for the synthesis of piano-stool Ir(III) cyclopentadienyl Schiff-base complexes as potential antibacterial agents. Using 15 picolinaldehydes (**A**–**O**), 24 amines (**1**–**24**), and four Cp/Cp* iridium precursors (**Cp1**–**4**), a library of 1440 complexes was generated and screened directly from crude reaction mixtures in a direct-to-biology approach. Biological screening revealed pronounced activity against Gram-positive *Staphylococcus aureus*, particularly for biphenyl-substituted Cp (**Cp2**) complexes, while no activity was observed against Gram-negative bacteria. A subset of the compounds exhibited potent and selective antibacterial activity with low mammalian cell toxicity. Dose-response validation identified 4 promising hit candidates, of which **Ir15** displayed low-micromolar activity against a panel of Gram-positive pathogens, limited hemolysis, and moderate cytotoxicity. Initial mechanistic studies indicate that **Ir15** acts through a membrane-associated mode of action involving mild membrane depolarization without large pore formation, alongside changes in nucleoid morphology. Overall, this work establishes Ir(III)Cp Schiff-base complexes as a modular antibacterial platform and identifies **Ir15** as a promising lead compound for further optimization.



KEYWORDS: *combinatorial synthesis, metalloantibiotics, iridium, Schiff-base, antibacterial, direct-to-biology*

INTRODUCTION

Antimicrobial resistance (AMR) is one of the most pressing health challenges of the 21st century and is associated with 4.71 million deaths in 2021 alone, including 1.14 million deaths directly caused by resistant bacterial infections.[1] It is forecasted to be the one of the leading causes of mortality by 2050, with approximately 10 million annual deaths. Projections estimate up to 2.4 million deaths in high-income countries from 2015 to 2050, and up to 5.2 million deaths in the Western Pacific region between 2023 and 2030 without proper preventative measures.[2,3] Among the WHO's 2024 priority pathogens, Gram-positive bacteria methicillin-resistant *Staphylococcus aureus* (MRSA) and vancomycin-resistant *Enterococcus faecium* (VRE) have been designated as high priority.[4,5] In light of these escalating resistance threats, the conventional antibacterial discovery pipeline, largely reliant on traditional organic medicinal chemistry, has produced limited success in recent decades. As of February 2025, 90 antibacterial agents containing at least one new therapeutic entity are in clinical development worldwide, comprising both traditional and non-traditional agents. However, between December 2023 and February 2025, only four new antibiotics were approved and just one advanced to the approval stage.[6] This insufficient progress underscores the urgent need to explore novel chemical spaces and alternative strategies in antibiotic discovery.

In 2015, The Community for Open Antimicrobial Drug Discovery (CO-ADD) was established as an open access platform enabling chemists around the world to submit their compounds to investigate previously underexplored chemical spaces for potential antibiotic discovery. The submitted compounds are evaluated against key bacterial and fungal pathogens to identify novel antimicrobial scaffolds.[7] As of 2020, more than 280,000 compounds had been submitted and tested, and among these compounds, considerable proportion do not meet the "usual drug-likeness" criteria (e.g Lipinski's Rule of Five[8]). One such compound class comprises metal

Received: May 25, 2026
Revised: September 1, 2026
Accepted: September 2, 2026

ACS Publications
© XXXX The Authors. Published by American Chemical Society

https://doi.org/10.1021/jacsau.6c00813
JACS Au XXXX, XXX, XXX−XXX

Downloaded from pubs.acs.org/jacsau/article-pdf/doi/10.1021/jacsau.6c00813/6856726/jacsau.6c00813.pdf by UNIV OF YORK user on 06 October 2026

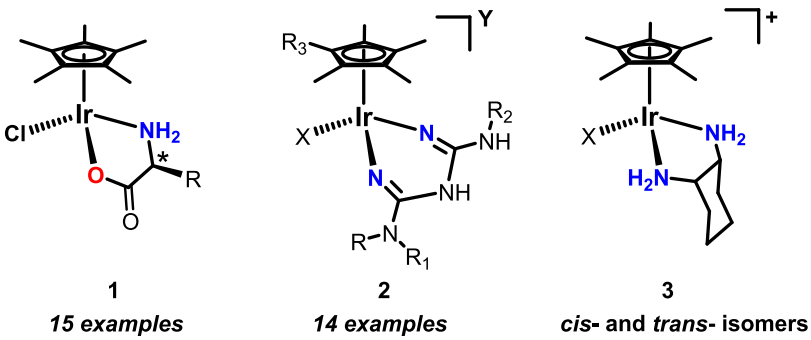


Figure 1. Selected iridium(III) cyclopentadienyl complexes from the literature.

complexes. A total of 906 metal complexes with 29 different metals had been submitted, and among these, 246 were active against bacterial strains with an extraordinary hit rate of 27%. On the other hand, the tested organic compounds only exhibited a hit-rate of 1.6%. The rate of antibacterial metal compounds without significant cytotoxicity against human cells was 9.9%, which is more than 10-fold higher than the general CO-ADD library (0.87%).[9]

Metal complexes expand chemical space beyond the constraints of organic drug scaffolds, which tend to be limited in three-dimensional character, by accessing more globular and structurally diverse structures, thereby enhancing the likelihood of engaging diverse biological targets.[10−12] Moreover, their unique chemical reactivity and functional properties, including ligand exchange, redox activity, and catalytic or metal-substitution processes, enable diverse and unconventional mechanisms of action.[13,14]

In the aforementioned CO-ADD study, iridium emerged as a promising metal center, with 33 evaluated complexes, of which five exhibited low cytotoxicity and high antimicrobial activity.[15] Diverse classes of iridium complexes have been investigated as potential antimicrobial agents.[16−28] In 2013, Simpson and co-workers investigated iridium N-heterocyclic carbene (NHC) complexes bearing charged moieties and evaluated their activity against a panel of Gram-positive and Gram-negative bacteria as one of the first examples of iridium scaffolds as potential antibacterials. Although promising antimicrobial activity was observed, cytotoxic activity down to 13.4 μM against L-929 Mouse Fibroblast cells remained a major limitation.[16] In parallel, piano-stool Ir(III) systems have been extensively studied due to their water solubility and well-tunable ligand environment.[29]

Piano-stool Ir(III) complexes have emerged as a promising class of antibacterial agents, exhibiting potent activity against drug-resistant pathogens such as MRSA, combined with low cytotoxicity, high stability, and reduced propensity for resistance development.[29−45] In 2013, Falkinham and co-workers established α-amino acid bearing iridium(iii) Cp complexes (Figure 1, **1**) as effective antibacterials against nontuberculous mycobacterium species.[30] Sadler and co-workers synthesized 14 iridium(III) complexes with different cyclopentadienyl derivatives, metformin or an *N*-substituted biguanide, and a halide ligand (Figure 1, **2**). Several of the complexes demonstrated selective and notable activity against Gram-positive bacteria, with minimum inhibitory concentrations (MICs) down to 0.5 μM. Additionally, the complexes exhibited stability in broth media and did not induce resistance development over 24 passages.[34] 1,2-diaminoalkane moiety-bearing iridium(III) Cp complexes have been reported as potent antibacterial agents against several resistant strains of *S. aureus*. The lead compound (Figure 1, **3**) exhibited MICs of 9.8 μM against *S. aureus* and 14.6 μM against MRSA. Notably, no hemolytic activity was observed in sheep red blood cells, and no cytotoxic effects were observed against Vero and Human embryonic kidney (HEK293) cells at concentrations at least 50-fold higher than the MIC values. Furthermore, the lead compound demonstrated low cytotoxicity in vivo and was evaluated in a mouse model following a single intravenous dose of 2.5 mg/kg.[36]

While the potential of metal complexes with diverse metal centers and ligand scaffolds as antimicrobial agents has been demonstrated in recent years, most current studies investigate only a small number of compounds at a time. This makes it inefficient and impractical to explore large libraries. Moreover, although promising compounds continue to be identified, our understanding of the relationships between their structure and antimicrobial activity remains limited.[43] Combinatorial chemistry offers a powerful solution by enabling the generation of structurally diverse large chemical libraries through the combination of building blocks using synthetic methodologies that are robust, adaptable, and highly efficient.[44] Iridium metal scaffolds have accessible oxidative states, +1 and +3, and have the versatility to coordinate with a wide range of donor ligands. These properties make it feasible to efficiently explore diverse chemical spaces by constructing large libraries of iridium complexes. Bernhard and co-workers pioneered combinatorial synthesis of luminescent iridium complexes back in 2004. They developed a library of 100 complexes by combining one neutral, 10 diamine-type and 10 different cyclometalating ligands to an iridium(III) metal center.[45] The same group expanded their approach and developed a library of 1152 iridium(III) compounds, which they screened as photocatalysts for the dehalogenation of aryl bromides.[46] More recently, the development of iridium(III) combinatorial libraries for biological applications has begun to attract attention. Vilar and co-workers have recently established a semi-automated synthesis platform for generating libraries of photo-cytotoxic heteroleptic iridium(III) complexes for potential use of photodynamic therapy (PDT).[47] By the same group, a combinatorial library of 78 phototoxic octahedral iridium(III) complexes with cyclometalating polyaromatic (CN) and phenanthroline-imidazole or dipyridophenazine derivatives (NN) ligands was established as a source of potential antibacterial agents.[48] Recently we established a combinatorial approach using CuAAc "Click" chemistry to synthesize 288 iridium complexes for antibacterial and photophysical evaluation.[49]

Downloaded from pubs.acs.org/jacsau/article-pdf/doi/10.1021/jacsau.6c00813/6856726/jacsau.6c00813.pdf by UNIV OF YORK user on 06 October 2026

https://doi.org/10.1021/jacsau.6c00813
JACS Au XXXX, XXX, XXX−XXX

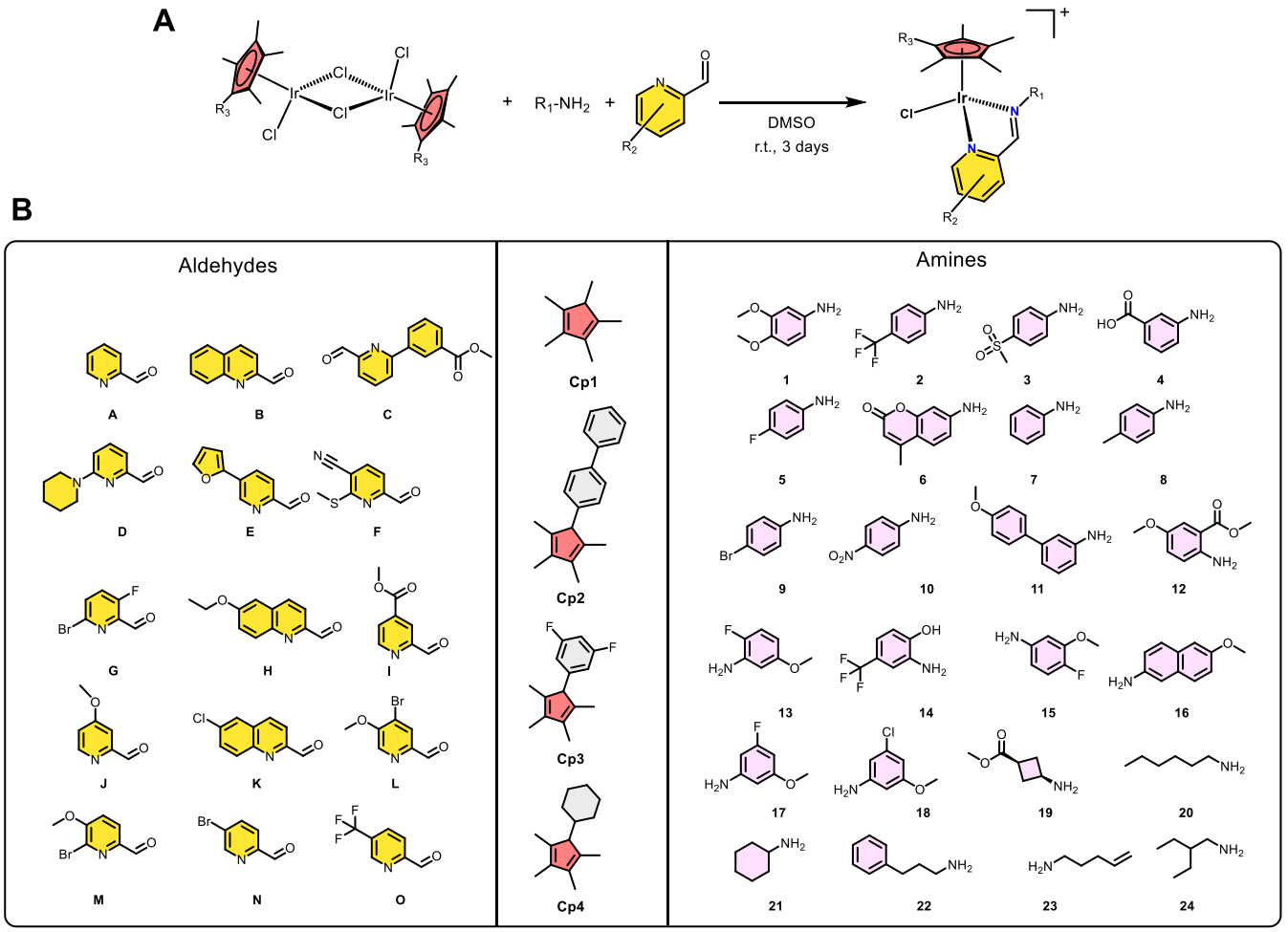


Figure 2. (A) General reaction scheme for the combinatorial synthesis of the iridium scaffolds. (B) Selected building blocks library consisting of 15 picolinaldehydes, 24 amines, and 4 Cp*/Cp derivatives.

Among the strategies explored in the literature, Schiff-base chemistry has emerged as particularly suitable for combinatorial metal complex synthesis due to its simplicity, modularity, and adaptability under mild reaction conditions. In 2014, the Ang group utilized a one pot metal-based three-component assembly (3CA) to develop water-soluble Ru-arene Schiff-base complexes. A library of 450 complexes was screened against different cancer cell lines.[50] This Schiff-base chemistry was further used by the same group to generate different ruthenium complex libraries and investigate their biological and catalytic properties.[51−54] In other work, Schiff-base complexes of a rhenium tricarbonyl scaffold were prepared in a combinatorial manner and tested for anticancer properties.[55,56]

The Schiff-base chemistry approach has recently been expanded by our group to synthesize 420 manganese(I) tricarbonyl complexes by combining 7 picolinaldehydes, 10 aniline derivatives and 6 axial ligands. The generated crude compound library was screened against MRSA, leading to the identification of 10 hit compounds. These hits were subsequently re-synthesized and evaluated against a panel of Gram-positive bacteria to confirm the reliability of their biological activity and to further expand their biological characterization. The lead compound exhibited low cytotoxicity against a human dermal fibroblast cell line, with a therapeutic index of 109.[43] Combinatorial chemistry provides a powerful platform for exploring diverse chemical spaces. These requirements are further accentuated in direct-to-biology approaches[57−60] which enable rapid screening of compound libraries without purification. Consequently, high-yielding reactions in biocompatible solvents are essential to allow the direct application of crude reaction mixtures in biological assays.

Inspired by the success of iridium complexes as antibiotics and their compatibility with combinatorial approaches, we sought to develop an operationally simple and broadly applicable synthetic platform. We herein report a one-pot, three-component strategy for the synthesis of a library of piano-stool Ir(III) Cp Schiff base complexes as potential antibacterial scaffolds. Initially, a commercially available pentamethylcyclopentadienyl (Cp*) iridium precursor was combined with 15 structurally diverse picolinaldehydes and 24 amines to evaluate the scope and efficiency of the methodology (Figure 2). To further enhance structural diversity and introduce an additional dimension of variation, we synthesized three tetramethylcyclopentadienyl (**Cp2-4**) derivatives and their corresponding iridium dimers, expanding the library to a total of 1440 compounds. Following the initial biological screening of the library, three hit compounds were identified and resynthesized for further validation and initial mode of action studies.

https://doi.org/10.1021/jacsau.6c00813
JACS Au XXXX, XXX, XXX−XXX

Downloaded from pubs.acs.org/jacsau/article-pdf/doi/10.1021/jacsau.6c00813/6852726/jacsau.6c00813.pdf by UNIV OF YORK user on 06 October 2026

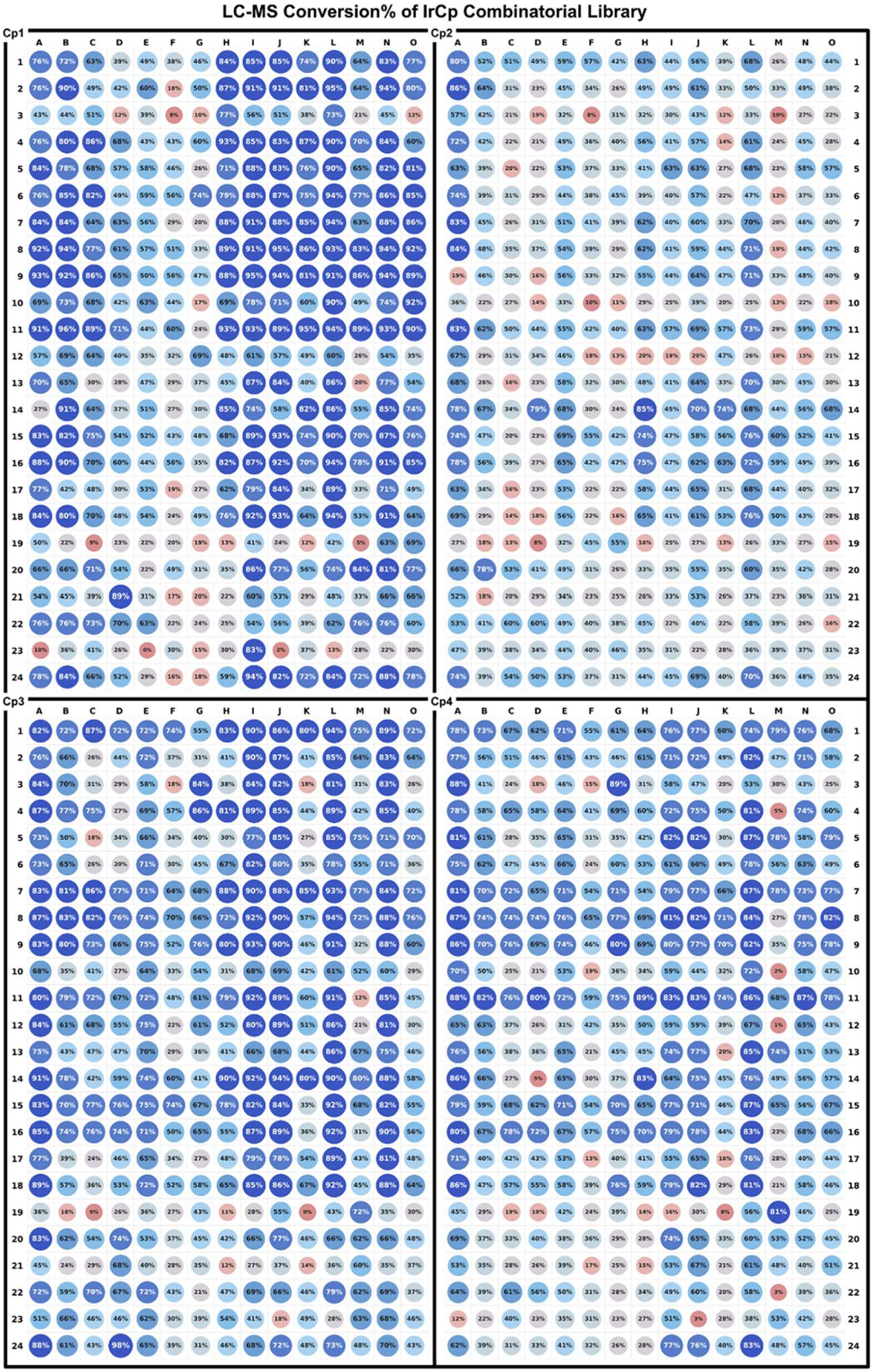


Figure 3. Conversion rates of the metal complex libraries determined as LC-MS peak area percentages at 254 nm (top left: **Cp1**; top right: **Cp2**; bottom left: **Cp3**; bottom right: **Cp4**). Compound peaks were automatically identified based on the target ion mass, and the corresponding UV signals were integrated using custom Python scripts (see Supporting Information for details). Reported conversions represent the combined signal of the parent ion (M^+) and the MeCN adduct $(M + MeCN)^{2+}$.

Downloaded from pubs.acs.org/jacsau/article-pdf/doi/10.1021/jacsau.6c00813/6852726/jacsau.6c00813.pdf by UNIV OF YORK user on 06 October 2026

https://doi.org/10.1021/jacsau.6c00813
JACS Au XXXX, XXX, XXX−XXX

RESULTS AND DISCUSSION

Combinatorial Synthesis of Ir(III) Cp Library

Successful combinatorial chemistry in drug development relies on the use of diverse and modular building blocks that enable efficient access to broad chemical space, thereby enhancing the likelihood of identifying active compounds. Concurrently, the synthetic methodology must be robust, scalable, and broadly tolerant of functional groups, while operating under mild conditions. Reactions should proceed with minimal side reactions and require little to no purification, ensuring suitability for high-throughput synthesis, characterization, and screening.[61] Schiff-base combinatorial chemistry has been pioneered by Ang and his co-workers as a facile and robust methodology for one pot 3CA combinatorial chemistry.[50] The promising antibacterial activity of IrCp complexes reported by the Sadler group,[34] together with the versatile combinatorial approach developed by Ang and co-workers,[50] inspired us to expand the approach to the synthesis of iridium-based scaffolds. Initially, a test reaction was conducted using **IrCp1**, an iridium complex synthesized from a commercially available pentamethylcyclopentadienyl (Cp*) precursor.[62] After reacting the iridium dimer with a model aniline and picolinaldehyde derivative for 3 days under ambient conditions, LC-MS indicated a promising conversion to the target complex. Following the successful test reaction, we selected a building block library based on availability and structural diversity (Figure 2). A protocol was developed using an Opentrons OT-2 liquid handling robot to dispense DMSO stock solutions of all building blocks into the corresponding wells of the 96 well plates. The reaction plates were allowed to stand for 3 days (without stirring or shaking), yielding a combinatorial library of 360 **IrCp1** complexes. After establishing the initial compound library, the structural diversity was further expanded through the incorporation of modified Cp ligands. (Figure 2). Ligands **Cp2-4** were synthesized via Grignard reactions (see SI for the detailed procedure). Notably, iridium(III) cyclopentadienyl complexes bearing biphenyl moieties (**Cp2**) were first reported by the Sadler group to exhibit potent anticancer activity,[63] and had previously been reported as effective antibacterial agents.[34] The substituents for **Cp3** and **Cp4** were selected to increase lipophilicity, which is known to enhance membrane permeability and cellular uptake.[64] Iridium half-sandwich dimers (**IrCp2** and **4**) were efficiently synthesized via microwave irradiation, following a reported procedure analogous to that used for **IrCp1**.[62] The dimer bearing bis(fluorophenyl) substituents (**IrCp3**) could not be obtained under the established conditions, which may be attributed to the strongly electron-withdrawing nature of the fluorine substituents. Such substituents are known to reduce ligand donor ability, potentially weakening metal-ligand interactions and increasing the energy barrier for complexation.[65] To synthesize the **IrCp3** dimer, the precursor was reacted in the microwave for 16 h at 132 °C and successfully precipitated from the reaction mixture. With the new IrCp dimers in hand we successfully expanded the combinatorial library to a total of 1440 Ir(III) Cp Schiff-base complexes.

LC-MS Characterization of the Combinatorial Library

The identity and purity of the crude reaction mixtures were assessed by LC-MS. Target masses were extracted using custom Python scripts, and the corresponding UV signals at 254 nm were integrated to determine relative peak areas. The average conversion of the library varied substantially with the Cp moiety (Figures 3 and S14). The variation in average conversion across the Cp series implies the strong dependence of scaffold formation efficiency on ligand structure. The Cp* derivative **Cp1** gave the highest average conversion (62 ± 25%), consistent with the well-established stabilizing effect of the electron-rich and sterically balanced Cp* ligand.[66] **Cp3** also exhibited similarly high average conversion (61 ± 22%), suggesting that its substitution pattern remains compatible with efficient complex formation despite increased structural modification of the Cp ring. By contrast, **Cp2**, bearing a biphenyl substituent, showed the lowest average conversion (42 ± 18%). This relatively lower yield may arise from the greater steric hindrance and conformational rigidity[67] of the biphenyl group, which could obstruct coordination or reduce the efficiency of complexation. **Cp4**, containing a cyclohexyl substituent, displayed intermediate conversion (55 ± 21%), indicating that the bulky but more flexible aliphatic substituent is better tolerated than the rigid aromatic biphenyl group, although still less effective than **Cp1** and **Cp3**. Overall, these data suggest that both steric profile and substituent electronics of the Cp ligand play an important role in determining the efficiency of iridium scaffold formation. With regards to the aldehyde building blocks, steric bulk in the 6-position resulted in generally lower average conversion rates (Figure S14). Conversely, aldehydes with no substitution at the 6-position have significantly higher average conversion rates. Within the amine building blocks two trends are visible. Firstly, aliphatic amines tend to give lower conversion rates. Strong electron withdrawing groups seem to negatively affect conversion rates as well. On the other hand, simple or bicyclic anilines seem to lead to very high conversions (Figure S14).

Single-Dose Response Biological Activity of the Combinatorial Library

We initially screened the 1440 compound crude IrCp Schiff base library against *S. aureus* at 12.5 and 50 μM, and against *E. coli* at 50 μM. These were selected as representative Gram-positive and Gram-negative bacteria strains, respectively, to enable assessment of antibacterial activity across different cellular membrane structures. Notably, none of the compounds within the library exhibited activity against *E. coli* at 50 μM which is in line with previously found trends indicating that most metal-based and organic compounds[68] are not able to penetrate Gram-negative bacteria.[9] For the **Cp1** library, we observed that only a minority of compounds (26%) was active at 50 μM, while only 2.5% of compounds exhibited measurable activity at 12.5 μM (Figures 5A and S14). In contrast, all compounds bearing the **Cp2** ligand completely inhibited *S. aureus* growth at 50 μM, and nearly 70% exhibited antibacterial activity at 12.5 μM. The superior antibacterial activity of biphenyl substituted (**Cp2**) Cp iridium(III) complexes was also observed by Sadler and co-workers.[34] The observed difference in activity may be attributed to the increased lipophilicity and rigidity of the biphenyl moiety, which could facilitate improved uptake through the bacterial membrane.[64] The majority of the **Cp3** library was active against *S. aureus* at 50 μM, however, only 42% exhibited complete growth inhibition at 12.5 μM (Figure S15). When we consider **Cp4** complexes, 91% were active at 50 μM, whereas only 26% inhibited the bacterial growth at 12.5 μM (Figure S15). At the level of individual building blocks, the aldehyde component exerts a dominant influence on antibacterial activity, with

Downloaded from pubs.acs.org/jacsau/article-pdf/doi/10.1021/jacsau.6c00813/6856726/jacsau.6c00813.pdf by UNIV OF YORK user on 06 October 2026

https://doi.org/10.1021/jacsau.6c00813
JACS Au XXXX, XXX, XXX−XXX

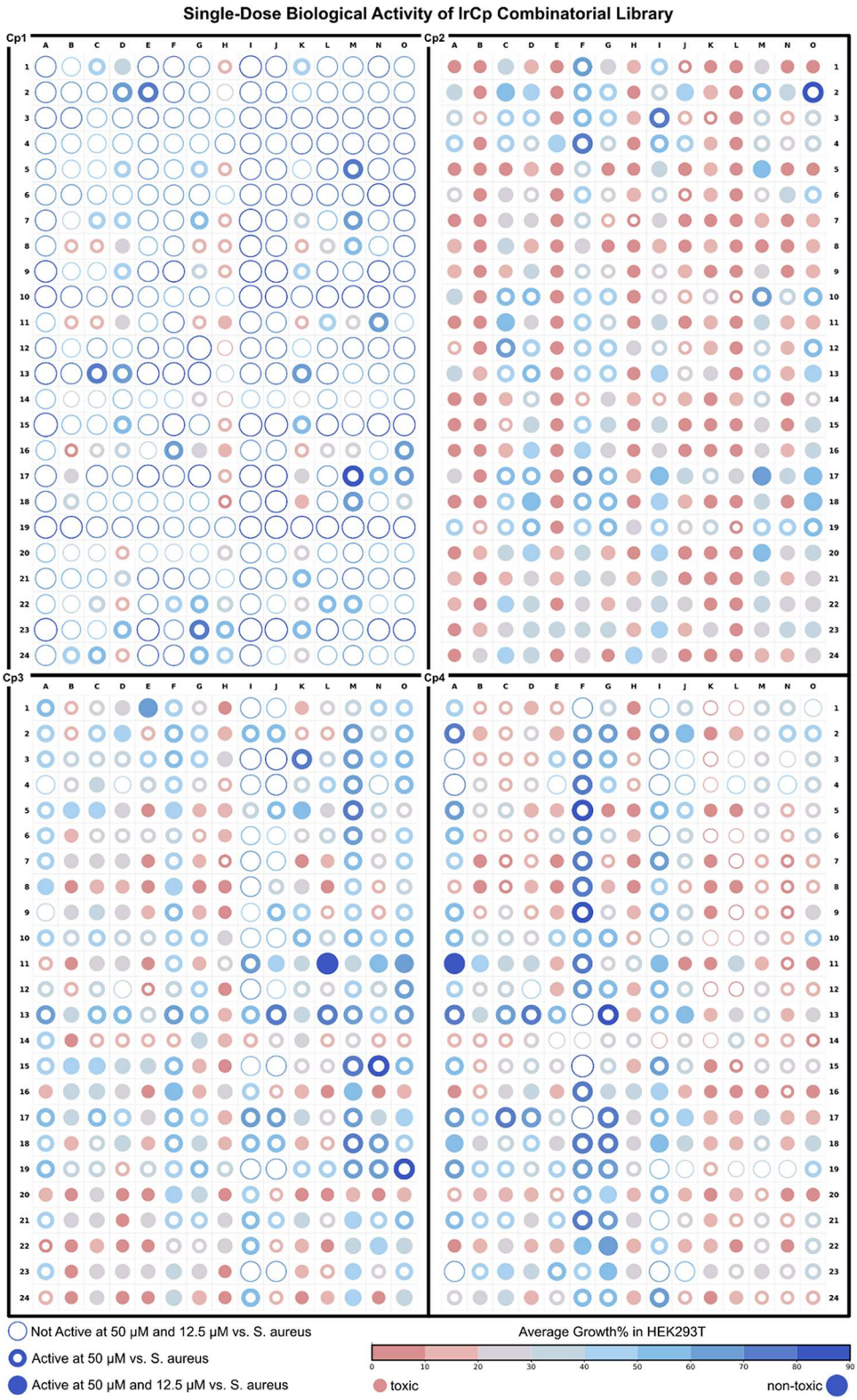


Figure 4. Single-dose biological characterization of the combinatorial library against *S. aureus* CCUG 62707 (top left: **Cp1**; top right: **Cp2**; bottom left: **Cp3**; bottom right: **Cp4**). Filled circles indicate measurable antibacterial activity at both 50 μM and 12.5 μM. Small white circles denote compounds that are active only at 50 μM, while empty circles indicate no detectable activity against *S. aureus* under the tested conditions. The color intensity corresponds to the single dose cytotoxic activity against HEK293T cells. The circle size is proportional to viability of HEK293T cells.

several aldehydes consistently associated with high levels of growth inhibition across multiple Cp cores and amines. In particular, aldehydes **B** (quinoline), **E** (furan-2-yl), **H** (ethoxy-quin), and **K** (chloro-quin) exhibit the highest rates of activity at 12.5 μM, with 50−70% of compounds containing these building blocks being active (Figures 5A and S15). These most active aldehydes share extended aromatic and heteroaromatic motifs, suggesting that increased π-interactions and hydro-

Downloaded from pubs.acs.org/jaaucr/article-pdf/doi/10.1021/jacsau.6c00813/6852726/jacsau.6c00813.pdf by UNIV OF YORK user on 06 October 2026

https://doi.org/10.1021/jacsau.6c00813
JACS Au XXXX, XXX, XXX−XXX

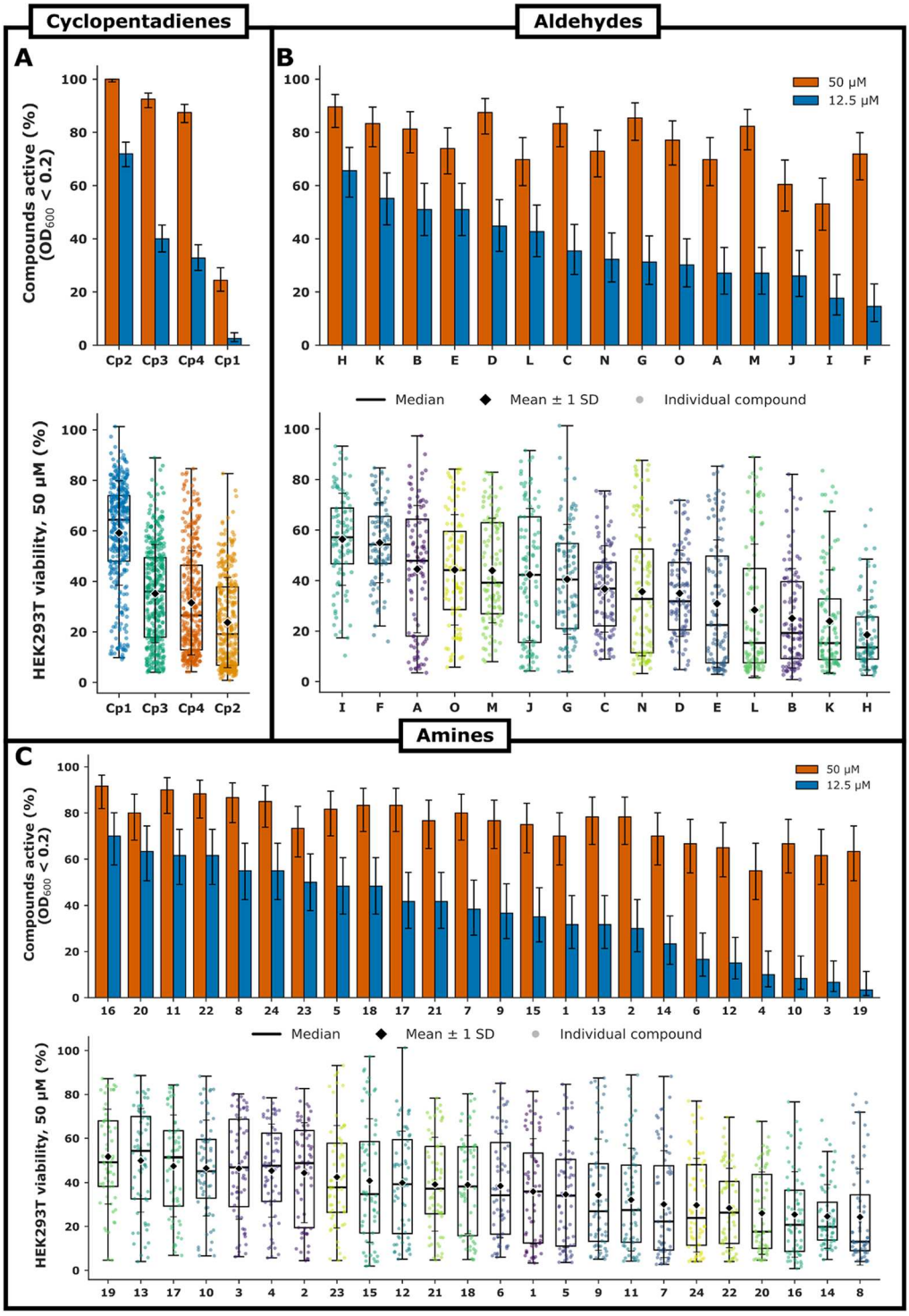


Figure 5. Activity distribution of the building blocks. (A) Antibacterial activity distribution of compounds across cyclopentadiene moieties against *S. aureus* at 50 μM (red) and 12.5 μM (blue), and HEK293T cell viability at 50 μM. (B) Antibacterial activity distribution of compounds across aldehyde moieties against *S. aureus* at 50 μM (red) and 12.5 μM (blue), and HEK293T cell viability at 50 μM. (C) Antibacterial activity distribution of compounds across amine moieties against *S. aureus* at 50 μM (red) and 12.5 μM (blue), and HEK293T cell viability at 50 μM.

phobic character contribute to enhanced antibacterial performance. In contrast, fewer than 30% of compounds with aldehydes **A** (pyridine), **F** (*o*-thiomethoxy-*m*-nitrile), **I** (*p*-methoxycarbonyl), **J** (*p*-methoxy), and **M** (*o*-bromo-*m*-methoxy) display activity at 12.5 μM (Figures 5A and S15). These lower-activity aldehydes are monocyclic pyridines and incorporate more polar functionality. These observations are consistent with the hypothesis that increased hydrophobicity and structural rigidity facilitate more effective interaction with bacterial membranes or intracellular targets.[69,70] In comparison, the amine component exerts a more moderate effect on antibacterial activity. Amines **8** (*p*-methyl), **11** (*m*-methoxyphenyl), **16** (6-methoxynaphthyl), **20** (hexyl), **22** (propanphenyl), **23** (pentenyl) and **24** (2-ethylbutan) are consistently

https://doi.org/10.1021/jacsau.6c00813
JACS Au XXXX, XXX, XXX−XXX

Downloaded from pubs.acs.org/jacsau/article-pdf/doi/10.1021/jacsau.6c00813/6852726/jacsau.6c00813.pdf by UNIV OF YORK user on 06 October 2026

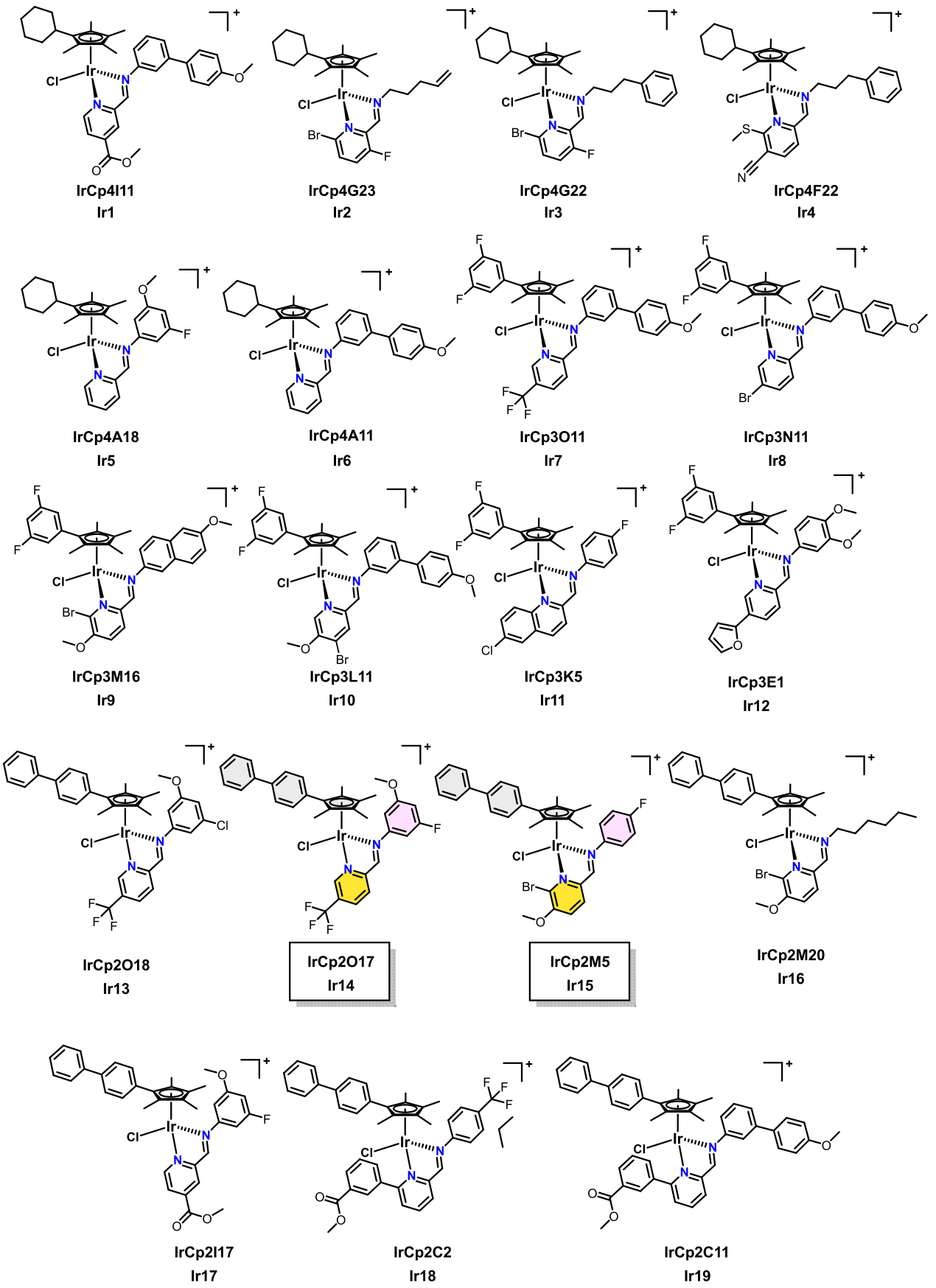


Figure 6. Selection of lead compounds from the initial screening library for dose-response biological characterization. A total of 19 compounds were selected based on their antibacterial activity against *S. aureus* at 12.5 μM. Compounds were further filtered to retain those maintaining >50% single dose (50 μM) viability in HEK293T cells.

https://doi.org/10.1021/jacsau.6c00813
JACS Au XXXX, XXX, XXX−XXX

Downloaded from pubs.acs.org/jaaucr/article-pdf/doi/10.1021/jacsau.6c00813/6852726/jacsau.6c00813.pdf by UNIV OF YORK user on 06 October 2026

Table 1. Selected 19 Hit Compounds from the Single-Dose Biological Assays[a]

compound		% Conv.	MIC (μM)			CC_{50} (μM)	TI
			S. aureus	*E. coli*	*E. coli* + PMBN	HEK293T	
Ir1	**IrCp4I11**	83	50	>100	100	65 ± 4	1.3
Ir2	**IrCp4G23**	23	25	>100	100	50 ± 3	2
Ir3	**IrCp4G22**	28	25	>100	100	47 ± 2	1.9
Ir4	**IrCp4F22**	31	12.5	>100	25	24 ± 9	1.9
Ir5	**IrCp4A18**	86	100	>100	>100	58 ± 8	0.6
Ir6	**IrCp4A11**	88	25	>100	>100	19 ± 1	0.8
Ir7	**IrCp3O11**	45	25−50	>100	100	23 ± 8	0.5
Ir8	**IrCp3N11**	85	25	>100	100	23 ± 9	0.9
Ir9	**IrCp3M16**	31	12.5	>100	>100	50 ± 20	4.0
Ir10	**IrCp3L11**	91	6.25	>100	25	15 ± 3	2.4
Ir11	**IrCp3K5**	27	25	>100	100	31 ± 10	1.2
Ir12	**IrCp3E1**	72	50	>100	>100	32 ± 6	0.6
Ir13	**IrCp2O18**	28	12.5	>100	50	45 ± 14	3.6
Ir14	**IrCp2O17**	32	6.25	>100	25	33 ± 8	5.3
Ir15	**IrCp2M5**	23	12.5	>100	50	51 ± 12	4.1
Ir16	**IrCp2M20**	35	6.25	>100	12.5	42 ± 8	6.7
Ir17	**IrCp2I17**	45	25	>100	>100	64 ± 20	2.6
Ir18	**IrCp2C2**	31	50−100	>100	100	>120	>2.4
Ir19	**IrCp2C11**	50	12.5−50	>100	25	33 ± 8	0.7

[a]%Conv. is the conversion percentage, determined via LC-MS. MIC values are given in μM, and determined against *S. aureus* CCUG 62707, and *E. coli* NCTC 13476. PMBN was used as an outer membrane permeabilizer at a sublethal concentration (10 μg/mL). Cytotoxicity was determined against Human Embryonic Kidney cells (HEK293T) and is given as CC_{50}. Therapeutic index (TI) is given as the ratio of CC_{50} and MIC against *S. aureus*. Experiments were performed in three biological replicates, each measured in triplicate.

associated with higher activity, with 50−70% of compounds active at 12.5 μM (Figures 5C and S16). On the other end, compounds with amines **3** (*p*-sulfonyl), **4** (*m*-carboxy), **6** (coumarin), **10** (*p*-nitro), **12** (*o*-methoxycarbonyl-*p*-methoxy), **14** (*o*-hydroxy-*m*-trifluoromethyl) and **19** (methyl 3-amino-cyclobutane-1-carboxylate) only show activity in a minority of the cases (3-23%, Figure S16). Structurally, amines with increased aromatic character or flexible hydrophobic substituents have higher activity-rates, whereas lower-activity amines tend to be more polar or electron poor. Overall, antibacterial activity is strongly dependent on the Cp scaffold, with the **Cp2** (biphenyl) series showing the highest potency, followed by **Cp3** and **Cp4**, while **Cp1** is largely inactive. Activity is primarily driven by the aldehyde component, with more hydrophobic, aromatic motifs enhancing potency, whereas the amine plays a secondary role, with hydrophobic substituents generally improving activity.

Following the single-dose evaluation of antibacterial activity, the cytotoxicity of the crude compounds was assessed against HEK293T cells at 50 μM. This *in vitro* kidney cell line is widely regarded as a gold-standard tool for nephrotoxicity screening in drug discovery, as the kidneys are a primary target of chemically induced injury and play a crucial role in drug excretion.[71] For the iridium library with the **Cp1** moiety, viability ranged from 9−100% (mean 59%, median 65%), with 70% of compounds achieving ≥50% viability, indicating a shift toward higher viability (Figures 4, 5A, and S19). In contrast, the **Cp2** library showed lower viability overall, ranging from 0.8−83% (mean 24%, median 19%), with only 2% of compounds achieving ≥50% viability. Both **Cp3** and **Cp4** libraries shifted toward higher viability (Figures 4, 5, and S19). **Cp3** showed viability of 0.2−89% (mean 30%, median 28%), with ∼20% of compounds achieving ≥50% viability, while **Cp4** ranged from 4−85% with slightly higher overall viability (mean 32%, median 27%) and 22% of compounds achieving ≥50% viability. These data reveal a clear dependence of cytotoxicity on the Cp core, with **Cp1** affording the highest overall viability and **Cp2** the lowest, while **Cp3** and **Cp4** display intermediate cytotoxicity profiles (Figures 4, 5, and S19). Aldehydes associated with strong antibacterial activity, (**B**, **E**, **K**, **H**) consistently correspond to lower average cell viability in the range of 18−31%. In contrast, aldehydes associated with lower antibacterial activity (**A**, **F**, **I**, **J**, and **M**) result in significantly higher viability (42−56%), indicating reduced cytotoxicity (Figures 5B and S19). The picture is slightly less clear with the amine building blocks where overall mean cell viability ranges from 24-52% (Figures 5C and S21). In general, amines with higher rates of antibacterial activity also have lower mean cell viability, suggesting that the aldehydes have a stronger influence on the cytotoxicity profile of the resulting compounds (Figures 4, 5, S20 and S21).

While a large number of compounds that showed significant antibacterial activity also displayed high toxicity, there was a small subset of compounds that retained antibacterial activity at 12.5 μM while maintaining ≥50% HEK293T cell viability, indicating the presence of a selectivity window within the library. Although such combinations are relatively rare, their consistent occurrence demonstrates that antibacterial activity and cytotoxicity are not strictly coupled within this scaffold. These "balanced" compounds are predominantly observed within **Cp2-4**.

At the aldehyde level, these combinations are most frequently associated with aldehydes with high average cell viability percentages (**A**, **F**, **I**, and **M**) and a few representing lower viability ones (**E**, **K**, **L**, and **N**) (Figures 4, 5, and S20). Amongst the amines, **11** stands out as it appears most frequently in selective compounds (Figures 6 and S21). In general, the occurring amines are on the lower end of the mean cell viability with **5**, **11**, **16**, **20**, and **22** all coming in below 35% (Figures 4, 5, and S21). This may suggest that for

Downloaded from pubs.acs.org/jacsau/article-pdf/doi/10.1021/jacsau.6c00813/6852726/jacsau.6c00813.pdf by UNIV OF YORK user on 06 October 2026

https://doi.org/10.1021/jacsau.6c00813
JACS Au XXXX, XXX, XXX−XXX

compounds with balanced properties the antibacterial contribution stems from the amine while the aldehyde seems to drive the non-toxic component.

Dose-Response Biological Activity of Selected Complexes

A subset of 19 compounds (Figure 6) that achieved growth inhibition at 12.5 μM against *S. aureus* while maintaining ≥50% HEK293T viability was selected from the library for dose-response validation. At this point, to confirm that the antibacterial activity of our crude mixtures originates from the putative complexes themselves, we examined the antibacterial activity of all 15 picolinaldehydes, 24 amines (Table S5) and 4 IrCp dimers (Table S5). With the exception of the **IrCp2** dimer (MIC = 12.5 μM), none of the building blocks exhibited any antibacterial activity up to 100 μM indicating that any activity observed from the crude reaction mixtures likely originates from the targeted Schiff-base iridium(III) metal complex.

We screened these 19 compounds against *S. aureus* and *E. coli* in dose-dependent assays. Most of the selected compounds exhibited good antibacterial activity against *S. aureus* with MIC values ranging from 6.25 to 100 μM. This is in line with what was seen during the initial screening of the library. Among these, **Ir4**, **Ir9**, **Ir10**, **Ir13**, **Ir14**, **Ir15**, and **Ir16** emerged as the most active derivatives. Notably, **Ir10**, **Ir14**, and **Ir16** displayed the highest potency, each exhibiting MIC values of 6.25 μM, (Table 1).

No antibacterial activity against *E. coli* was observed for any of the compounds at concentrations up to 100 μM. However, enhanced activity was detected in the presence of the membrane permeabilizer polymyxin B nonapeptide (PMBN).[72] Unlike polymyxin B, PMBN does not possess intrinsic antibacterial activity, making it a valuable adjuvant for use in combination therapies.[73] In particular, the MIC of **Ir16** against *E. coli* was reduced from >100 μM down to 12.5 μM in the presence of PMBN. This observation indicates that the lack of activity against Gram-negative bacteria is likely attributable to limited uptake or increased efflux across the outer membrane, rather than an absence of intrinsic antibacterial potency (Table 1).

The cytotoxicity of the compounds was evaluated in HEK293T cells in a dose-dependent manner, revealing a broad range of CC_{50} (CC_{50} is the compound concentration that reduces cell viability by 50%) values and highlighting notable differences in selectivity across the series. Several compounds exhibited moderate to high cytotoxicity, with CC_{50} values below 30 μM, including **Ir4**, **Ir6**, **Ir7**, **Ir8**, and **Ir10**. Importantly, some of the most promising antibacterial compounds maintained a favorable balance between potency and cytotoxicity. **Ir9**, **Ir14**, **Ir15**, and especially **Ir16** exhibited relatively high CC_{50} values (50 ± 20 μM, 33 ± 8 μM, 51 ± 12 μM, and 42 ± 8 μM, respectively) in combination with promising MIC values, resulting in the highest therapeutic indices (TI = 4.0, 5.3, 4.1, and 6.7, respectively) (Table 1). The dose-dependent cytotoxicity assays were conducted with an incubation time of 24 h, which is comparable with the incubation time used in antibacterial assays (16 h). We believe that results in the fairest comparison of the two biological assays. These compounds therefore represent the most selective candidates within the series and were selected for batch synthesis, purification, and subsequent hit validation.

Batch Synthesis of Selected Complexes

Following single-dose and dose-response assays, four iridium(III) complexes, **Ir9**, **Ir14**, **Ir15**, and **Ir16**, were selected for scale-up synthesis and purification. The synthesis followed a generally similar procedure. Briefly, the iridium dimer (0.5 equiv) was combined with the corresponding amine (1 equiv) and aldehyde (1 equiv) in DCM/MeOH (1:1) and stirred at room temperature overnight. Upon completion, excess *n*-hexane was added to precipitate the product, which was subsequently isolated and purified by flash column chromatography on silica. Although **Ir16** was identified as the most promising compound in the dose-response assays, repeated attempts to purify this complex were unsuccessful. Multiple purification strategies were explored, including column chromatography under varying stationary phases and solvent systems, recrystallization attempts, and repeated washing procedures. Complexes **Ir9**, **Ir14** and **Ir15** were synthesized and isolated successfully with 27%, 45%, and 47% yield respectively. Compound purity and identity was confirmed by LC-MS and NMR characterization, and high-resolution mass spectra (HRMS).

Antibacterial Activity of Lead Complexes: Hit Validation

To validate the antibacterial activity observed in the crude mixtures, the purified complexes **Ir9**, **Ir14** and **Ir15** were re-screened against *S. aureus*. We observed that pure **Ir9** was not soluble in various biological growth media at the testing concentrations and therefore it was excluded from further biological evaluation. Notably, the antibacterial activity of **Ir15** increased following purification, with the MIC decreasing from 12.5 μM to 3.13 μM (Table 2), whereas the activity of **Ir14** unexpectedly diminished with the MIC increasing from 6.25 μM to 25 μM (Table S6, **A**). Crude LC-MS analysis provides an explanation for the observed activity difference of **Ir14**, showing multiple species (Figures S56 and S57) in the crude mixture compared to the cleaner profile of **Ir15** (Figures S58

Table 2. Antibacterial Activity of Ir15 against Gram-Positive (*S. aureus* CCUG 62707, MRSA (JE2), *S. aureus* (SH1000), *S. epidermidis* TU3298, and *Bacillus subtilis* MW168, *Enterococcus feacium* CUG 19434, and *Enterococcus faecalis* CCUG 19916T) and Gram-Negative Panel (*Escherichia coli* NCTC 134376, *Actinobacteria baumannii* AB5075)[a]

antibacterial activity of **Ir15**			
strain		**Ir15**	control
S. aureus	CCUG 62707	3.13−6.25	0.86
	JE2	1.56−3.13	
	SH1000	3.13	
S. epidermidis	TU3298	3.13	0.86
B. subtilis	MW168	3.13−6.25	0.22
E. faecium	CUG 19434	6.25	0.86
E. faecalis	CCUG 19916T	6.25	0.43
E. coli	NCTC 13476	>100	≤0.01
		12.5*	
A. baumannii	AB5075	50	0.03
		12.5*	

[a]*Indicates the presence of sublethal concentration (10 μg/mL) of PMBN, outer membrane permeabilizer. Control is positive control antibiotic Vancomycin (VCM) for Gram-positive, Polymyxin B (PMB) for Gram-negative. MIC values are given in μM. Experiments were performed in three biological replicates, each measured in triplicate.

Downloaded from pubs.acs.org/jacsau/article-pdf/doi/10.1021/jacsau.6c00813/6856726/jacsau.6c00813.pdf by UNIV OF YORK user on 06 October 2026

https://doi.org/10.1021/jacsau.6c00813
JACS Au XXXX, XXX, XXX−XXX

and S59). The reduced antibacterial activity upon purification suggests that the biological activity of the crude sample is not solely attributable to the target complex, but rather that the active species may be present only in the crude mixture. Based on these findings, **Ir15** was selected for further biological characterization and subsequently screened against an expanded panel of Gram-positive strains. **Ir15** demonstrated promising antibacterial activity across the Gram-positive panel, with MICs in the low micromolar range. Against *S. aureus*, **Ir15** exhibited strain-dependent activity, with MIC values ranging from 1.56−6.25 μM. Comparable activity was observed against *S. epidermidis* and enterococci species (Table 2). In line with the results from the crude reaction screening, **Ir15** displayed limited antibacterial activity against Gram-negative strains, with no measurable activity against *E. coli* (MIC >100 μM) and only moderate activity against *A. baumannii* (MIC = 50 μM). However, upon treatment with sublethal concentrations of PMBN a notable enhancement in activity was observed (12.5 μM for both *E. coli* and *A. baumannii*, Table 2). This indicates that **Ir15** possesses intrinsic activity against Gram-negative bacteria but is unable to efficiently penetrate the outer membrane.

Next, we investigated if the bacterial growth inhibition stems from a bacteriostatic or bactericidal effect. We determined the minimum bactericidal concentration (MBC) of the purified lead complexes (**Ir14** and **Ir15**) against *S. aureus*. For both complexes, the MBC values were found in the same range as MIC values, and, since the MBC/MIC ratio is lower 4, the compounds can be classified as bactericidal.[74]

Hemolytic and Cytotoxic Properties of Lead Complexes

The ability of antibacterial compounds to selectively target bacteria while minimizing cytotoxic effects on mammalian cells is essential. Therefore, cytotoxicity of the lead compounds was reevaluated against the HEK293T mammalian cell line. **Ir14** displays high cytotoxicity, with a CC_{50} value of 13 ± 4 μM. Notably, this result is not in an agreement with that observed in the crude mixture single-dose screening and dose-response assays, where **Ir14** did not display comparable cytotoxicity. The lower CC_{50} value in conjunction with the higher MIC for **Ir14** also results in a reduced selectivity (TI = 0.5). **Ir15** exhibits a CC_{50} value of 48 ± 4 μM (Table 3) which is consistent with the one measured in the crude reaction mixture (CC_{50} = 51 ± 12 μM). This indicates a moderate effect on mammalian cell viability. The TI was found to be between 8−31 (CC_{50} value over MIC values against *S. aureus* strains). Notably, the selectivity of **Ir15** improved, with a TI increase from 4.1 to 8−15 upon purification. It demonstrates the ability of **Ir15** retain antibacterial efficacy while maintaining an acceptable safety margin under the tested conditions.

Table 3. Cytotoxicity of Ir14 and Ir15 against HEK293T and Human Red Blood Cells[a]

	toxicity assays		
	CC_{50}	HC_{10}	HC_{50}
Ir14	13 ± 4	64 ± 13	125 ± 9
Ir15	48 ± 4	124 ± 7	141 ± 5

[a]CC_{50}, HC_{10}, and HC_{50} values were given in μM.

Crude LC-MS analysis provides an explanation for the observed cytotoxicity difference of **Ir14**, showing multiple species (Figures S55 and S56) in the crude mixture compared to the cleaner profile of **Ir15** (Figures S57 and S58). The enhanced cytotoxicity upon purification suggests that the biological activity of the crude sample is not solely attributable to the isolated parent complex. Rather, the less cytotoxic species may be present only in the crude mixture, and purification revealed the intrinsic toxicity of **Ir14**. To further assess the cytotoxic properties of the lead complexes, 10% and 50% hemolytic concentrations (HC_{10} and HC_{50}) were determined using human red blood cells (RBC). **Ir14** shows relatively higher hemolytic activity with HC_{10} value 64 ± 13 (Table 3), while **Ir15** exhibits very low hemolytic activity with HC_{10} values 124 ± 7 μM, 20-40 times higher than MIC value (Table 3).

Taken together, these findings emphasize the importance of follow-up validation of crude screening hits and demonstrate that **Ir15** represents a more favorable candidate, combining retained antibacterial activity with a more consistent and moderate cytotoxicity profile. While crude library screening provides an efficient starting point for exploring and narrowing down chemical space, these results highlight the necessity of subsequent validation using purified compounds to accurately assess biological activity and cytotoxicity. Overall, **Ir15** shows promising antibacterial activity against a broad panel of Gram-positive pathogens, does not cause significant hemolysis and exhibits only minor toxicity against mammalian cells, showcasing a favorable therapeutic window.

Stability of Ir15

We started to investigate the stability of the lead compound by investigating whether pre-incubation of **Ir15** in the bacterial growth medium (MH) would affect its antibacterial activity. Standard serial dilution plates were prepared, and bacteria were added either immediately or after 24 h of incubation under MIC assay conditions. For the replicate inoculated immediately, the MIC remained 3.13−6.25 μM, consistent with previous results. However, when bacteria were added after 24 h, antibacterial activity was significantly reduced, with an MIC of 50 μM. These results indicate that, although **Ir15** is sufficiently stable to produce consistent antibacterial effects across replicates and bacterial strains, it undergoes some type of speciation or degradation in MH medium within 24 h (Table S3). Followingly, we extended the stability studies to different biologically relevant solvent systems by measurement of UV/Vis absorbance at 37 °C over 20 h (Figure S1). In DMSO and DMSO:H_2O (1:1) **Ir15** exhibited good stability, with no significant decrease in absorbance over the measured period (Figure S2A,B and Table S2). In contrast, significant changes in the UV/Vis spectrum were observed in both H_2O (Figure S2C and Table S2) and PBS (1X) (Figure S2D and Table S2). A clear decline in absorbance was detected over time, suggesting degradation of the complex. As we observed degradation of **Ir15** under certain conditions, we further investigated the stability of the compound *via* LC-MS in DMSO:H_2O, H_2O, and PBS over 20 h. In H_2O **Ir15** exhibits degradation, primarily driven by chloride dissociation and subsequent ligand substitution with acetonitrile (MeCN) in the mobile phase, and formation of the $[(M - Cl) + MeCN]^{2+}$ complex (Figure S5). Notably, after 6 h, the emergence of two dimeric IrCp species was observed (Figures S7 and S8). Although degradation was also observed in the DMSO:H_2O mixture, a significant fraction of the parent complex remained detectable even after 21 h (Figure S11). However, LC-MS analysis showed that **Ir15** exhibits good stability in PBS where

Downloaded from pubs.acs.org/jacsau/article-pdf/doi/10.1021/jacsau.6c00813/6856726/jacsau.6c00813.pdf by UNIV OF YORK user on 06 October 2026

https://doi.org/10.1021/jacsau.6c00813
JACS Au XXXX, XXX, XXX−XXX

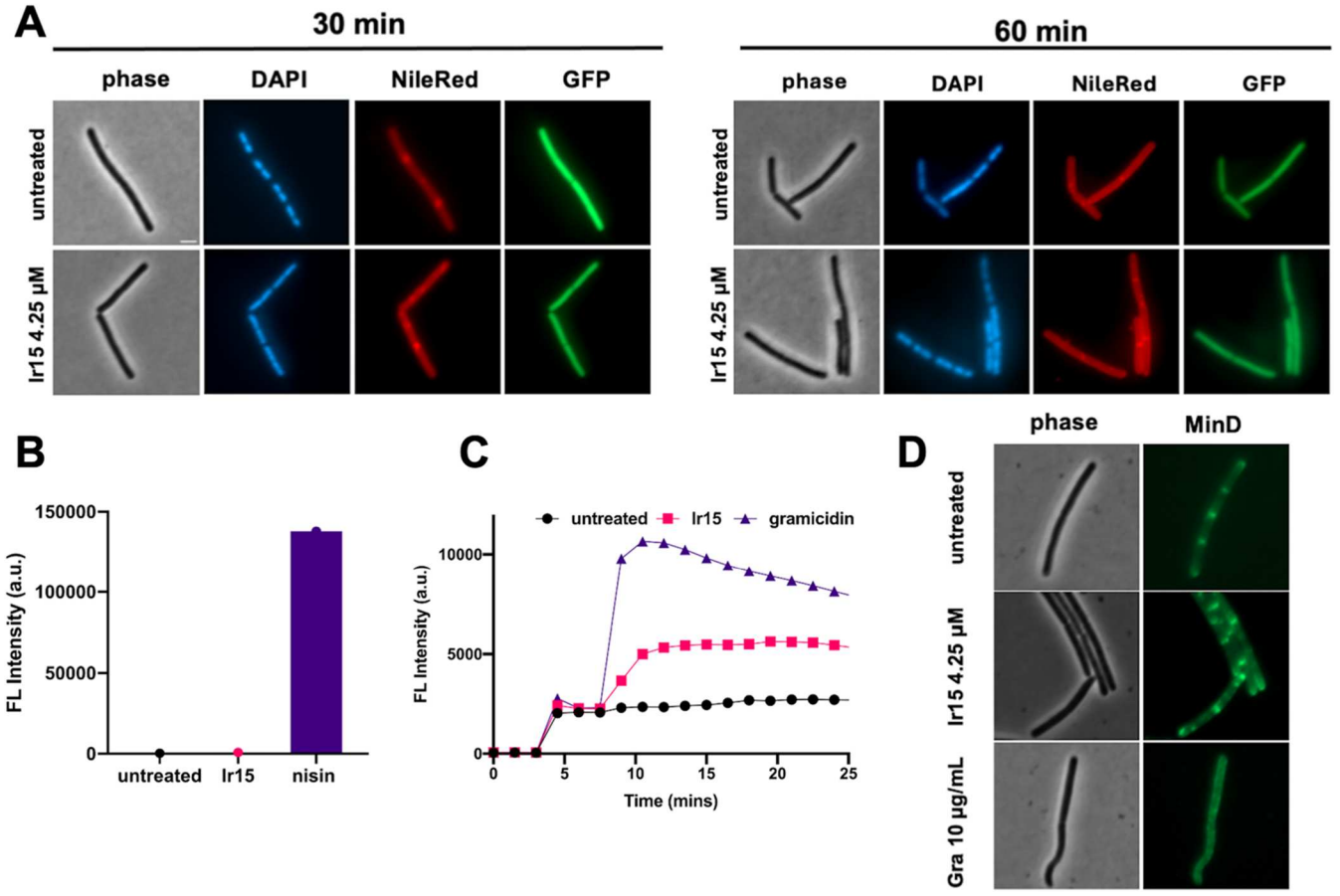


Figure 7. Initial mode of action of **Ir15**, hit compound. (A) Bacterial cytological profiling of *B. subtilis* bSS82, constitutively expressing GFP from the *PrpsD* promoter, stained with Nile red (membrane) and DAPI (DNA) after 30 and 60 min of incubation. (B) Propidium Iodide staining of *B. subtilis* 168CA (pore formation assay). 1.6 μg/mL nisin was used as positive control. (C) $DiSC_3(5)$ assay in *B. subtilis* 168CA (membrane depolarization assay). 1 μg/mL gramicidin was used as positive control. (D) Localization of MinD-GFP in *B. subtilis* TB35 (*Pxyl-gfp-minD*). Localization of MinD depends on the membrane potential. 10 μg/mL gramicidin was used as positive control. All assays were performed after treatment with 4.25 μM **Ir15**. Scale bar 2 μm.

most of the parent complex remains intact (Figures S12 and S13). This is likely due to the high chloride concentration in PBS (137 mM), preventing chloride dissociation from the parent complex.[75] Finally, we evaluated the stability of **Ir15** in human blood plasma at 37 °C to obtain a preliminary insight into its behavior under physiological conditions. Briefly, **Ir15** was incubated in human plasma for either 0, 6, or 24 h, the protein precipitated and supernatant analyzed by LC-MS. Benzyl benzoate was used as the internal standard. From the data it is clear that a portion of **Ir15** reacts with the blood plasma as the amount of compound at $t = 0$ is 55−27% lower than a unreacted sample of the same concentration. The wide range suggests that a quick reaction happens upon contact with blood plasma which is sensitive to the exact timing of sample handling. Conversely 24−29% of **Ir15** are detected after 6 h and 9−11% after 24 h highlighting that while the compound is degrading over time a portion remains intact. Notably, the antibacterial activity as well as cytotoxicity of **Ir15** was consistent across biological replicates, indicating that the complex retains sufficient stability under biological conditions to exert its activity.

Mode of Action

Encouraged by the promising biological characteristics of **Ir15**, we conducted initial mode of action investigations of this compound class with phenotypic analysis in the Gram-positive model organism *B. subtilis*. To this end, we first confirmed the MIC against *B. subtilis* 168CA, the background strain of our reporter construct. Here, **Ir15** exhibited comparable antibacterial activity, with an MIC value of 3.13−6.25 μM (Table 2). Based on the MIC value, we determined the optimal stressor concentration (OSC) in acute shock experiments. The OSC is defined as the concentration that reduces bacterial growth by 50−70% during the mid-exponential phase, thereby applying sufficient stress to induce a clear phenotype without causing excessive cell death or lysis that could obscure primary effects of the compound.[76] The growth curve analysis (Figure S26) identified an OSC of 4.25 μM.

To get an overview of the cellular effects of the compounds, we employed bacterial cytological profiling (BCP).[77] To this end, we used a strain intracellularly expressing green-fluorescent protein (GFP) from the strong, constitutive *PrpsD* promoter (*B. subtilis* bSS82), stained with the membrane dye Nile red and the DNA dye 4′,6-diamidino-2-phenylindole (DAPI). Combined with phase contrast microscopy, this setup allows simultaneous assessment of cell morphology, cell lysis, pore formation, membrane morphology, and nucleoid morphology in one assay.[76]

Upon treatment with **Ir15**, no apparent differences in overall cell morphology (phase contrast) or membrane integrity

https://doi.org/10.1021/jacsau.6c00813
JACS Au XXXX, XXX, XXX−XXX

Downloaded from pubs.acs.org/jaacsu/article-pdf/doi/10.1021/jacsau.6c00813/6852726/jacsau.6c00813.pdf by UNIV OF YORK user on 06 October 2026

(GFP) were observed (Figure 7A). Notably, we observed Nile Red foci formation, indicating mild membrane stress. These results suggest that although membrane integrity remains largely unaffected, the antibacterial activity of **Ir15** likely involves membrane-related mechanisms.

A substantial effect of **Ir15** was observed on the bacterial nucleoid (DAPI), showing visible changes in its morphology (Figure 7A). Particularly, after 60 min of treatment, the phenotype points towards compromised DNA integrity which can indicate DNA fragmentation or other structural changes.[78]

Cell Envelope Stress

The Nile Red staining suggested that **Ir15** may exert partial membrane-associated activity. To further investigate this, we examined whether it facilitates the passage of molecules smaller than GFP across the cell membrane.[76] As a first step, we assessed the uptake of the membrane-impermeable, red-fluorescent dye propidium iodide (PI). In these experiments **Ir15** did not result in increased PI uptake, confirming that it does not form large pores (Figure 7B).

In contrast, membrane depolarization was observed using the potentiometric fluorescent dye 3,3′-dipropylthiadicarbocyanine iodide ($DiSC_3(5)$)[79] (Figure 7C), indicating that **Ir15** induces ion translocation and disrupts membrane polarization. This finding was independently confirmed by assessing the localization of the cell division regulation protein MinD, which localizes at the midcell and poles in healthy cells, but delocalizes into membrane-associated clusters upon loss of membrane potential (Figure 7D).[80] Here, **Ir15** induces a mild delocalization of MinD after 30 min of treatment. Taken together, these results demonstrate that **Ir15** induces membrane stress by disrupting membrane polarization, while not causing large pore formation or detectable structural damage to the cellular membrane.

DNA Binding Properties

DAPI staining revealed that **Ir15** induces alterations in bacterial nucleoid structure after 60 min of treatment (Figure 7A). To further investigate this effect, we sought to assess the DNA-binding properties of the compound by performing an MIC shift assay in the presence of difference concentrations of calf-thymus DNA. While the positive control Actinomycin D, an antibiotic known to interact with GC-rich DNA sequences,[81] exhibits decreasing antibacterial activity with increasing concentration of DNA, the MIC of **Ir15** remains unchanged (Figure S24). To specifically evaluate a possible DNA interaction mechanism, an ethidium bromide (EtBr) fluorescence displacement assay was performed. In this assay, EtBr intercalates into DNA, resulting in a strong fluorescence signal.[82,83] Upon addition of a competing DNA interacting agent, EtBr is displaced from the DNA duplex, leading to a decrease in fluorescence intensity. Treatment of the calf thymus DNA-Ethidium complex with serial dilutions of **Ir15**, showed only minimal interaction (5% displacement) at concentrations corresponding to the MIC. Noticeable displacement of EtBr (45−50%) was only observed at the highest concentration tested (200 μM, Figure S25), indicating that **Ir15** does not interact with DNA in a manner that would displace EtBr (such as e.g., intercalation) at biologically relevant concentrations.

MIC in Glucose-Defined Medium

To better mimic physiological conditions and assess whether the lead compound is taken up via active or passive transport, MIC assays were conducted in glucose-defined M9 medium. We observed that *S. aureus* failed to grow under these conditions as reported in the literature,[84] hence the medium was supplemented with 10% (v/v) TSB to support bacterial growth. MIC values against *S. aureus* remain unchanged under standard experimental conditions in glucose-defined M9 growth medium (Table S8). This suggests that the antibacterial activity of the lead compound is not strongly dependent on nutrient conditions implying that uptake is not strictly dependent on energy-driven transport processes. Antibacterial activity is often governed by permeability and efflux rather than active transport alone, and passive diffusion mechanisms can contribute to the transport across cellular membrane.[85]

Determination of Synergy with Clinically Relevant Antibiotics

We next expanded our study to explore the mode of action of the lead compound and to determine whether **Ir15** can synergistically interact with clinically relevant antibiotics. We conducted a combination study with checkerboard assays using four different antibiotics (vancomycin, ciprofloxacin, chloramphenicol and kanamycin) against our Gram-positive model organism *S. aureus* (CCUG 62707). Neither synergistic nor antagonistic effects were observed with any of the tested antibiotics, indicating that the mode of growth inhibition of **Ir15** is unrelated to that of other antibiotics (Figure S18).

Reactive Oxygen Species

Metal complexes often induce oxidative stress (ROS) in cells, which can significantly contribute to membrane and DNA damage, mostly through generation of hydroxyl radicals.[86] Although iridium cannot replace iron or copper in a Fenton reaction to create hydroxyl radicals from hydrogen peroxide, a cyclometalated iridium(iii) complex has been shown to increase intracellular reactive oxygen species formation.[87] Notably, we previously demonstrated that iridium Cp complexes can catalyze transfer hydrogenation reactions;[49] this redox activity may further disrupt cellular redox balance, thereby promoting ROS accumulation.[88] Bacterial cells contain high amounts of iron and the Fenton reaction is a common source of hydroxyl radicals.[89] To asses if bacterial growth inhibition of **Ir15** involves reactive oxygen species, a scavenger assay was employed. In this modified MIC assay, the activity of a test compound is determined in (i) scavenger-free medium, (ii) medium containing the superoxide scavenger tiron, (iii) the hydroxyl radical scavenger thiourea, and (iv) a mix of both. In case the mode of action involves ROS formation, an increase of the MIC value is expected in the medium containing the scavenger specific to the ROS that is generated. In our case, MIC values against *B. subtilis* 168CA in the presence of tiron remain unchanged, whereas we unexpectedly obtained a 2-fold lower MIC value (1.56−3.13 μM) in the presence of thiourea (Table S9). This led us to do further investigations to determine if thiourea modulates the antibacterial activity of **Ir15**. A checkerboard synergy assay against *B. subtilis* 168CA was initially performed (Figure S28). The interaction between thiourea and **Ir15** was evaluated using the fractional inhibitory concentration index (FICI), calculated based on MIC values defined as $OD_{600} \leq 0.1$. Across six independent replicates, the mean FICI was 0.47 ± 0.11, indicating an overall trend toward synergistic interaction.[90] However, variability between replicates was observed, with FICI values spanning the synergy-additive boundary. This

Downloaded from pubs.acs.org/jacsau/article-pdf/doi/10.1021/jacsau.6c00813/6856726/jacsau.6c00813.pdf by UNIV OF YORK user on 06 October 2026

https://doi.org/10.1021/jacsau.6c00813
JACS Au XXXX, XXX, XXX−XXX

suggests that while the combination might exhibit a synergistic effect, there is variability across the replicates. A checkerboard synergy assay was also performed against *S. aureus* (Figure S29) with a mean FICI of 0.53 ± 0.16, indicating an overall trend toward additive interaction.[90] Finally, because the proposed mechanism of action of our lead compound involves mild membrane depolarization, we examined whether thiourea enhances disruption of membrane polarization. A $DiSC_3(5)$ assay performed in the presence of thiourea against *B. subtilis* 168CA showed no change in the membrane depolarization profile (Figure S26). Overall, while thiourea does not potentiate membrane depolarization, it contributes to moderately enhance antibacterial activity, resulting predominantly in additive effects.

CONCLUSION

Iridium(III) complexes have been identified as promising antibacterial compounds in the literature. In parallel, combinatorial chemistry provides a powerful and efficient strategy to generate large, structurally diverse libraries, enabling rapid screening while allowing systematic investigation of structure-activity relationships. This strategy facilitates the identification of molecular features that drive antibacterial activity and enables the optimization of lead compounds. In this work, we have applied a robust and operationally simple one-pot, three-component combinatorial strategy for the rapid generation of structurally diverse piano-stool Ir(III)Cp Schiff-base complexes. By combining 15 picolinaldehydes, 24 amines, and four cyclopentadienyl iridium scaffolds, we generated a library of 1440 complexes and demonstrated that this approach is compatible for direct-to-biology antibacterial screening. This platform enables efficient exploration of the metal-based chemical space and provides a scalable route toward the identification of novel antibacterial scaffolds.

Crude libraries were analyzed by LC-MS, and conversion rates were calculated through custom processing scripts. The combinatorial workflow proved sufficiently robust to generate a large and chemically diverse library amenable to biological evaluation. This further highlights the compatibility of Schiff-base chemistry with high-throughput synthesis of organometallic compounds.

Biological screening of the crude library revealed a clear dependence of antibacterial activity and cytotoxicity on the Cp scaffold and structure of other building blocks.

While many compounds exhibiting strong antibacterial activity also displayed cytotoxicity, a subset retained antibacterial activity while maintaining high mammalian cell viability, demonstrating the presence of a selectivity window within the libraries. These findings emphasize the importance of balancing hydrophobicity and structural features to optimize both potency and selectivity.

From this dataset, 19 compounds were selected for dose-response validation, leading to the identification of four candidates (**Ir9**, **Ir14**, **Ir15**, and **Ir16**) with low-micromolar antibacterial activity against *S. aureus*. These were pursued for resynthesis and purification. However, **Ir9** exhibited poor solubility in MH and DMEM media, while **Ir16** could not be successfully purified. Consequently, hit validation studies were carried out with **Ir14** and **Ir15**. Notably, the comparison between crude and purified samples highlighted the importance of downstream validation, as exemplified by **Ir14**, where apparent activity in crude mixtures could not be fully attributed to the isolated complex. This observation emphasizes that direct-to-biology screening, while powerful, must be complemented by hit validation with the purified compounds to accurately determine biological activity.

Ir15 demonstrated consistent antibacterial activity across a panel of Gram-positive pathogens, including MRSA, *S. epidermidis*, and enterococci species, with MIC values in the low micromolar range. Importantly, **Ir15** displayed only moderate cytotoxicity and low hemolytic activity, resulting in a favorable therapeutic index of 8−31. The compound exhibited only limited activity against Gram-negative bacteria. However, this activity was significantly enhanced in the presence of sublethal concentration of polymyxin B nonapeptide, indicating that outer membrane permeability is a key barrier to activity rather than an absence of intrinsic antibacterial potency.

Mechanistic investigations provided an initial insight into the mode of action of **Ir15**. Bacterial cytological profiling of *B. subtilis* revealed that the compound induces mild membrane stress, without causing large pore formation or complete membrane disruption. This is further supported by the delocalization of MinD, consistent with loss of membrane potential. In parallel, alterations in nucleoid morphology were observed after 60 min of incubation, suggesting an additional intracellular effect. However, DNA-binding studies, including MIC shift and ethidium bromide displacement assays, did not support direct DNA intercalation as the primary mechanism. Furthermore, ROS scavenger assays indicated that oxidative stress is unlikely to be the dominant driver of antibacterial activity. Taken together, these initial results suggest a mode of action involving membrane depolarization and downstream intracellular effects, rather than a single molecular target.

Stability studies revealed that **Ir15** remains stable in DMSO, DMSO:H_2O and PBS but undergoes gradual degradation in aqueous environments. LC-MS stability analysis revealed that degradation happens through chloride dissociation and aquation. Nevertheless, sufficient stability is retained over the time scale of biological assays to enable reproducible antibacterial activity. The observed stabilizing effect of chloride-rich environments, such as PBS, further highlights the importance of solution conditions in modulating the behavior of these complexes.

Overall, this study demonstrates that combinatorial organometallic chemistry, combined with direct-to-biology screening, represents a powerful strategy for metalloantibiotic discovery. By enabling rapid access to large and diverse libraries, this approach facilitates the identification of active and selective compounds within large chemical space that would be difficult to explore using conventional synthetic methods.

Future work will focus on further optimization of the lead scaffold to improve potency, selectivity, and stability, as well as to enhance activity against Gram-negative pathogens. The data obtained in this study can now be leveraged to train predictive machine learning models to guide library synthesis towards compounds with optimal biological properties. In addition, more detailed mechanistic studies will be required to fully elucidate the molecular targets and pathways involved in antibacterial mode of action. Expanding this combinatorial platform to other metal centers and ligand classes may further broaden the accessible chemical space and accelerate the discovery of next-generation antimicrobial agents.

Downloaded from pubs.acs.org/jacsau/article-pdf/doi/10.1021/jacsau.6c00813/6856726/jacsau.6c00813.pdf by UNIV OF YORK user on 06 October 2026

https://doi.org/10.1021/jacsau.6c00813
JACS Au XXXX, XXX, XXX−XXX

■ ASSOCIATED CONTENT

Data Availability Statement

The authors declare that all data supporting the current findings of this study are available in the main manuscript or in the associated Supporting Information. All numerical LC-MS (retention times and conversion%) and biological (Minimum inhibitory concentrations, HEK293T growth inhibition) data is supplied in an additional data file. The collated LC-MS spectra of all combinatorial libraries are supplied in an additional data file. The Python code used in automatic LC-MS data processing is accessible at the Frei Lab GitHub repository https://github.com/TheFreiLab/FreiLab-LCMSProcessing.

Supporting Information

The Supporting Information is available free of charge at https://pubs.acs.org/doi/10.1021/jacsau.6c00813.

Experimental details and LC-MS methods; solution stability and speciation studies of the hit compound Ir15; LC-MS-based conversion analysis and antibacterial activity broken down by cyclopentadienyl, aldehyde, and amine building blocks; checkerboard assays with clinically relevant antibiotics (vancomycin, kanamycin, ciprofloxacin, chloramphenicol); cytotoxicity (HEK293T) and hemolysis data including building-block analyses and dose-response curves for Ir14 and Ir15; DNA-interaction studies (CT-DNA MIC modulation and ethidium bromide displacement); and mechanistic investigations (optimal stressor concentration, $DiSC_3(5)$ membrane depolarization, and thiourea/tiron synergy assays in *B. subtilis* 168CA and *S. aureus* CCUG 62707) (PDF)

LCMS traces (PDF)

Full compound characterization is provided, including processed LC-MS spectra of crude complexes, ^{1}H, ^{13}C and ^{19}F NMR spectra, GC-MS data, and HRMS for the ligand building blocks and isolated complexes (XLSX)

■ AUTHOR INFORMATION

Corresponding Author

Angelo Frei − *Department of Chemistry, Biochemistry & Pharmaceutical Sciences, University of Bern, 3012 Bern, Switzerland; Department of Chemistry, University of York, York YO10 5DD, U.K.;* orcid.org/0000-0001-6169-2491; Email: angelo.frei@york.ac.uk

Authors

Çağrı Özsan − *Department of Chemistry, Biochemistry & Pharmaceutical Sciences, University of Bern, 3012 Bern, Switzerland; Department of Chemistry, University of York, York YO10 5DD, U.K.*

Athi Welsh − *Department of Chemistry, Biochemistry & Pharmaceutical Sciences, University of Bern, 3012 Bern, Switzerland; Department of Chemistry, University of York, York YO10 5DD, U.K.*

Stefano Zineddu − *Department of Chemistry "Ugo Schiff", University of Florence, Sesto Fiorentino 50019, Italy*

David R. Husbands − *Department of Chemistry, University of York, York YO10 5DD, U.K.;* orcid.org/0000-0001-8693-7766

Kiera Robinson − *Department of Chemistry, University of York, York YO10 5DD, U.K.*

Anson Kwok-Hei Chau − *Department of Chemistry, University of York, York YO10 5DD, U.K.*

Complete contact information is available at: https://pubs.acs.org/10.1021/jacsau.6c00813

Author Contributions

Conceptualization: Ç.Ö., A.F. Data Curation: Ç.Ö., A.W., D.R.H., A.F. Formal Analysis: Ç.Ö., A.W., S.Z.I. Funding Acquisition: A.F. Investigation: Ç.Ö., A.W., S.Z.I., K.R. Methodology: Ç.Ö., A.W., S.Z.I., D.R.H. Project Administration: A.F. Resources: A.F. Software and supervision: Ç.Ö., A.F. Validation: Ç.Ö. Visualization: Ç.Ö., D.R.H., A.F. Writing—original draft preparation: Ç.Ö., A.F. Writing—review and editing: Ç.Ö., A.F.

Notes

The authors declare no competing financial interest.

■ ACKNOWLEDGMENTS

We sincerely thank Prof. Anne-Kathrin Duhme-Klair for supporting our research group. Prof. Peter O'Toole and Dr. Grant Calder are acknowledged for giving the opportunity to use their microscope facility. We thank Prof. Ronan McCarthy for providing the bacterial strains. Dr. Jared Cartwright is acknowledged for giving the opportunity to use the lab facility to prepare bacteria for microscopy experiments, CHyM at the University of York for biolab access and Dr. Lianne Willems for the HEK293T cells. Blood was collected from anonymous voluntary donors at the University of York. A.F., A.W., D.R.H. and C.O. gratefully acknowledge funding from the Swiss National Science Foundation Ambizione grant PZ00P2_202016, a COST-Project Grant (IZCOZ0_220299, A.F.) and from a Research Partnership Grant and support by the University of Bern and York. The authors acknowledge the use of OpenAI ChatGPT, Anthropic Clause and Google Gemini to assist with drafting, refactoring and troubleshooting Python code used for data processing and figure generation. All code was reviewed, tested, edited and executed by the authors, who take full responsibility for the accuracy of the analyses and the content of the manuscript.

■ REFERENCES

(1) Naghavi, M.; Vollset, S. E.; Ikuta, K. S.; et al. Global burden of bacterial antimicrobial resistance 1990−2021: a systematic analysis with forecasts to 2050. *Lancet* **2024**, *404*, 1199−1226.

(2) Murray, C. J. L.; Ikuta, K. S.; Sharara, F.; et al. Global burden of bacterial antimicrobial resistance in 2019: a systematic analysis. *Lancet* **2022**, *399*, 629−655.

(3) Antimicrobial resistance expected to cause 5.2 million deaths in the Western Pacific by 2030. https://www.who.int/westernpacific/news/item/13-06-2023-antimicrobial-resistance-expected-to-cause-5.2-million-deaths-in-the-western-pacific-by-2030.

(4) Sati, H.; Carrara, E.; Savoldi, A.; et al. The WHO Bacterial Priority Pathogens List 2024: a prioritisation study to guide research, development, and public health strategies against antimicrobial resistance. *Lancet Infect. Dis.* **2025**, *25*, 1033−1043.

(5) Rajput, P.; Nahar, K. S.; Rahman, K. M. Evaluation of Antibiotic Resistance Mechanisms in Gram-Positive Bacteria. *Antibiotics* **2024**, *13*, No. 1197.

(6) Analysis of Antibacterial Agents in Clinical and Preclinical Development: Overview and Analysis 2025; https://www.who.int/publications/i/item/9789240113091.

(7) Cooper, M. A. A community-based approach to new antibiotic discovery. *Nat. Rev. Drug Discovery* **2015**, *14*, 587−588.

Downloaded from pubs.acs.org/jacsau/article-pdf/doi/10.1021/jacsau.6c00813/6852726/jacsau.6c00813.pdf by UNIV OF YORK user on 06 October 2026

(8) Lipinski, C. A.; Lombardo, F.; Dominy, B. W.; Feeney, P. J. Experimental and computational approaches to estimate solubility and permeability in drug discovery and development settings. *Adv. Drug Delivery Rev.* **1997**, *23*, 3−25.
(9) Frei, A.; Zuegg, J.; Elliott, A. G.; et al. Metal complexes as a promising source for new antibiotics. *Chem. Sci.* **2020**, *11*, 2627−2639.
(10) Lovering, F.; Bikker, J.; Humblet, C. Escape from Flatland: Increasing Saturation as an Approach to Improving Clinical Success. *J. Med. Chem.* **2009**, *52*, 6752−6756.
(11) Gasser, G.; Metzler-Nolte, N. The potential of organometallic complexes in medicinal chemistry. *Curr. Opin. Chem. Biol.* **2012**, *16*, 84−91.
(12) Morrison, C. N.; Prosser, K. E.; Stokes, R. W.; et al. Expanding medicinal chemistry into 3D space: metallofragments as 3D scaffolds for fragment-based drug discovery. *Chem. Sci.* **2020**, *11*, 1216−1225.
(13) Frei, A.; Verderosa, A. D.; Elliott, A. G.; Zuegg, J.; Blaskovich, M. A. T. Metals to combat antimicrobial resistance. *Nat. Rev. Chem.* **2023**, *7*, 202−224.
(14) Waters, J. E.; Stevens-Cullinane, L.; Siebenmann, L.; Hess, J. Recent advances in the development of metal complexes as antibacterial agents with metal-specific modes of action. *Curr. Opin. Microbiol.* **2023**, *75*, No. 102347.
(15) Frei, A.; Elliott, A. G.; Kan, A.; et al. Metal Complexes as Antifungals? From a Crowd-Sourced Compound Library to the First In Vivo Experiments. *JACS Au* **2022**, *2*, 2277−2294.
(16) Simpson, P. V.; Schmidt, C.; Ott, I.; Bruhn, H.; Schatzschneider, U. Synthesis, Cellular Uptake and Biological Activity Against Pathogenic Microorganisms and Cancer Cells of Rhodium and Iridium N-Heterocyclic Carbene Complexes Bearing Charged Substituents. *Eur. J. Inorg. Chem.* **2013**, *2013*, 5547−5554.
(17) Liao, G.; Peng, X.; Li, T.; et al. The Discovery of an Iridium(III) Dimer Complex as a Potent Antibacterial Agent against Non-Replicating Mycobacterium smegmatis. *Polymers* **2018**, *10*, No. 297, DOI: 10.3390/polym10030297.
(18) Gupta, A.; Prasad, P.; Gupta, S.; Sasmal, P. K. Simultaneous Ultrasensitive Detection and Elimination of Drug-Resistant Bacteria by Cyclometalated Iridium(III) Complexes. *ACS Appl. Mater. Interfaces* **2020**, *12*, 35967−35976.
(19) Hohlfeld, B. F.; Gitter, B.; Kingsbury, C. J.; et al. Dipyrrinato-Iridium(III) Complexes for Application in Photodynamic Therapy and Antimicrobial Photodynamic Inactivation. *Chem.- Eur. J.* **2021**, *27*, 6440−6459.
(20) Das, B.; Biswas, P.; Mallick, A. I.; Gupta, P. Application of Mono and Trinuclear Cyclometalated Iridium (III) Complexes in Differential Bacterial Imaging and Antimicrobial Photodynamic Therapy. *Chem. - Eur. J.* **2024**, *30*, No. e202400646.
(21) Moreth, D.; Stevens-Cullinane, L.; Rees, T. W.; et al. Antibacterial activity of Au(I), Pt(II), and Ir(III) biotin conjugates prepared by the iClick reaction: influence of the metal coordination sphere on the biological activity. *JBIC, J. Biol. Inorg. Chem.* **2024**, *29*, 573−582.
(22) Butuyuyu, B. J.; Liu, J.; Ding, Q.; et al. 808 nm Light-Triggered Cyanine-Decorated Iridium(III) Complexes for Antibacterial Photodynamic Therapy in Deep-Tissue. *Inorg. Chem.* **2025**, *64*, 8135−8142.
(23) Gautam, A.; Sasmal, P. K. Eradication of Antibiotic-Resistant Gram-Positive Bacteria and Biofilms by Rationally Designed AIE-Active Iridium(III) Complexes Derived from Cyclometalating 2-Phenylquinoline and Ancillary Bipyridyl Ligands. *Inorg. Chem.* **2025**, *64*, 2905−2918.
(24) Lu, Y.; Zhang, X.; Song, M.; et al. Tetrazolium iridium complexes as potential antibacterial agents. *RSC Adv.* **2025**, *15*, 2329−2333.
(25) Shu, J.; Jiang, H.; Lin, M.; et al. D-Alanine functionalized Iridium(III) complexes as two-photon photo-antibiotics for bacteria-specific ablation in infected macrophages. *Eur. J. Med. Chem.* **2025**, *294*, No. 117758.
(26) Paes, B. V.; Costa, D. N.; Esarev, I. V.; et al. A cyclometalated iridium(III) complex with 2-acetylpyridine-N(4)-ortho-chlorophenyl thiosemicarbazone: Potent antiproliferative and antibacterial activities. *J. Inorg. Biochem.* **2026**, *276*, No. 113179.
(27) Li, Y.; Zhou, C.; Liu, M.; et al. Cyclometalated Iridium(III) Complexes with eDNA-Degrading Activity for Combating Gram-Positive Bacterial Biofilms. *ACS Infect. Dis.* **2026**, *12*, 1409−1422.
(28) Zhang, Y.; Shao, L.; Wang, Z.; et al. Pyridine-containing iridium complexes as gram-negative bacteria specific therapeutic agents with low resistance development. *J. Inorg. Biochem.* **2026**, *279*, No. 113274.
(29) Bernier, C. M.; DuChane, C. M.; Martinez, J. S.; Falkinham, J. O. I.; Merola, J. S. Synthesis, Characterization, and Antimicrobial Activity of RhIII and IrIII N-Heterocyclic Carbene Piano-Stool Complexes. *Organometallics* **2021**, *40*, 1670−1681.
(30) Karpin, G. W.; Merola, J. S.; Falkinham, J. O. Transition Metal−α-Amino Acid Complexes with Antibiotic Activity against Mycobacterium spp. *Antimicrob. Agents Chemother.* **2013**, *57*, 3434−3436.
(31) Karpin, G. W.; Morris, D. M.; Ngo, M. T.; Merola, J. S.; Iii, J. O. F. Transition metal diamine complexes with antimicrobial activity against Staphylococcus aureus and methicillin-resistant S. aureus (MRSA). *Med. Chem. Commun.* **2015**, *6*, 1471−1478.
(32) Gajera, S. B.; Mehta, J. V.; Patel, M. N. Design of Multifunctional IridiumIII Compounds as a Potential Therapeutic Agents from Basic Molecular Scaffolds. *ChemistrySelect* **2016**, *1*, 3966−3973.
(33) Chellan, P.; Avery, V. M.; Duffy, S.; et al. Organometallic Conjugates of the Drug Sulfadoxine for Combatting Antimicrobial Resistance. *Chem. - Eur. J.* **2018**, *24*, 10078−10090.
(34) Chen, F.; Moat, J.; McFeely, D.; et al. Biguanide Iridium(III) Complexes with Potent Antimicrobial Activity. *J. Med. Chem.* **2018**, *61*, 7330−7344.
(35) DuChane, C. M.; Brown, L. C.; Dozier, V. S.; Merola, J. S. Synthesis, Characterization, and Antimicrobial Activity of RhIII and IrIII β-Diketonato Piano-Stool Compounds. *Organometallics* **2018**, *37*, 530−538.
(36) DuChane, C. M.; Karpin, G. W.; Ehrich, M.; Falkinham, J. O.; Merola, J. S. Iridium piano stool complexes with activity against *S. aureus* and MRSA: it is past time to truly think outside of the box. *Med. Chem. Commun.* **2019**, *10*, 1391−1398.
(37) Baartzes, N.; Jordaan, A.; Warner, D. F.; et al. Antimicrobial evaluation of neutral and cationic iridium(III) and rhodium(III) aminoquinoline-benzimidazole hybrid complexes. *Eur. J. Med. Chem.* **2020**, *206*, No. 112694.
(38) Mansour, A. M.; Radacki, K. Antimicrobial properties of half-sandwich Ir(III) cyclopentadienyl complexes with pyridylbenzimidazole ligands. *Dalton Trans.* **2020**, *49*, 4491−4501.
(39) Liu, X.; Shao, M.; Liang, C.; et al. Preparation and Bioactivity of Iridium(III) Phenanthroline Complexes with Halide Ions and Pyridine Leaving Groups. *ChemBioChem* **2021**, *22*, 557−564.
(40) Balázs, B.; Tóth, Z.; Kacsir, I.; et al. Targeting Multiresistant Gram-Positive Bacteria by Ruthenium, Osmium, Iridium and Rhodium Half-Sandwich Type Complexes With Bidentate Monosaccharide Ligands. *Front. Chem.* **2022**, *10*, No. 868234, DOI: 10.3389/fchem.2022.868234.
(41) Marco, A.; Vigueras, G.; Busto, N.; et al. Novel valproate half-sandwich rhodium and iridium conjugates to fight against multidrug-resistant Gram-positive bacteria. *Dalton Trans.* **2023**, *52*, 13482−13486.
(42) Sawkmie, M.; Banothu, V.; Kaminsky, W.; Kollipara, M. R. Antimicrobial study of ruthenium and iridium half-sandwich complexes containing fluorenyl hydrazonothiazole derivative ligands. *J. Coord. Chem.* **2023**, *76*, 1650−1665.
(43) Scaccaglia, M.; Birbaumer, M. P.; Pinelli, S.; Pelosi, G.; Frei, A. Discovery of antibacterial manganese(I) tricarbonyl complexes through combinatorial chemistry. *Chem. Sci.* **2024**, *15*, 3907−3919.
(44) Liu, R.; Li, X.; Lam, K. S. Combinatorial chemistry in drug discovery. *Curr. Opin. Chem. Biol.* **2017**, *38*, 117−126.
(45) Lowry, M. S.; Hudson, W. R.; Pascal, R. A.; Bernhard, S. Accelerated Luminophore Discovery through Combinatorial Synthesis. *J. Am. Chem. Soc.* **2004**, *126*, 14129−14135.

Downloaded from pubs.acs.org/jacsau/article-pdf/doi/10.1021/jacsau.6c00813/6856726/jacsau.6c00813.pdf by UNIV OF YORK user on 06 October 2026

(46) Mdluli, V.; Diluzio, S.; Lewis, J.; et al. High-throughput Synthesis and Screening of Iridium(III) Photocatalysts for the Fast and Chemoselective Dehalogenation of Aryl Bromides. *ACS Catal.* **2020**, *10*, 6977−6987.
(47) Kench, T.; Rahardjo, A.; Terrones, G. G.; et al. A Semi-Automated, High-Throughput Approach for the Synthesis and Identification of Highly Photo-Cytotoxic Iridium Complexes. *Angew. Chem., Int. Ed.* **2024**, *63*, No. e202401808.
(48) Kench, T.; Chowdhury, N. S.; Rahman, K. M.; Vilar, R. Discovery of Phototoxic Metal Complexes with Antibacterial Properties via a Combinatorial Approach. *Inorg. Chem.* **2025**, *64*, 5113−5121.
(49) Husbands, D. R.; Özsan, Ç.; Welsh, A.; Gammons, R. J.; Frei, A. High-throughput triazole-based combinatorial click chemistry for the synthesis and identification of functional metal complexes. *Nat. Commun.* **2025**, *16*, No. 11195.
(50) Chow, M. J.; Licona, C.; Wong, D. Y. Q.; et al. Discovery and Investigation of Anticancer Ruthenium−Arene Schiff-Base Complexes via Water-Promoted Combinatorial Three-Component Assembly. *J. Med. Chem.* **2014**, *57*, 6043−6059.
(51) Chow, M. J.; Alfiean, M.; Pastorin, G.; Gaiddon, C.; Ang, W. H. Apoptosis-independent organoruthenium anticancer complexes that overcome multidrug resistance: self-assembly and phenotypic screening strategies. *Chem. Sci.* **2017**, *8*, 3641−3649.
(52) Weng, C.; Shen, L.; Ang, W. H. Harnessing Endogenous Formate for Antibacterial Prodrug Activation by in cellulo Ruthenium-Mediated Transfer Hydrogenation Reaction. *Angew. Chem., Int. Ed.* **2020**, *59*, 9314−9318.
(53) Weng, C.; Yang, H.; Loh, B. S.; Wong, M. W.; Ang, W. H. Targeting Pathogenic Formate-Dependent Bacteria with a Bioinspired Metallo−Nitroreductase Complex. *J. Am. Chem. Soc.* **2023**, *145*, 6453−6461.
(54) Weng, C.; Shen, L.; Teo, J. W.; et al. Targeted Antibacterial Strategy Based on Reactive Oxygen Species Generated from Dioxygen Reduction Using an Organoruthenium Complex. *JACS Au* **2021**, *1*, 1348−1354.
(55) Konkankit, C. C.; Vaughn, B. A.; MacMillan, S. N.; Boros, E.; Wilson, J. J. Combinatorial Synthesis to Identify a Potent, Necrosis-Inducing Rhenium Anticancer Agent. *Inorg. Chem.* **2019**, *58*, 3895−3909.
(56) Konkankit, C. C.; Vaughn, B. A.; Huang, Z.; Boros, E.; Wilson, J. J. Systematically altering the lipophilicity of rhenium(I) tricarbonyl anticancer agents to tune the rate at which they induce cell death. *Dalton Trans.* **2020**, *49*, 16062−16066.
(57) Stevens, R.; Bendito-Moll, E.; Battersby, D. J.; et al. Integrated Direct-to-Biology Platform for the Nanoscale Synthesis and Biological Evaluation of PROTACs. *J. Med. Chem.* **2023**, *66*, 15437−15452.
(58) Wilders, H.; Biggs, G.; Rowe, S. M.; et al. Expedited SARS-CoV-2 Main Protease Inhibitor Discovery through Modular 'Direct-to-Biology' Screening. *Angew. Chem., Int. Ed.* **2025**, *64*, No. e202418314.
(59) Thomas, R. P.; Heap, R. E.; Zappacosta, F.; et al. A direct-to-biology high-throughput chemistry approach to reactive fragment screening. *Chem. Sci.* **2021**, *12*, 12098−12106.
(60) Kaguchi, R.; Katsuyama, A.; Sato, T.; et al. Discovery of Biologically Optimized Polymyxin Derivatives Facilitated by Peptide Scanning and In Situ Screening Chemistry. *J. Am. Chem. Soc.* **2023**, *145*, 3665−3681.
(61) Welsh, A.; Husbands, D.; Frei, A. High-Throughput Combinatorial Metal Complex Synthesis. *Angew. Chem., Int. Ed.* **2025**, *64*, No. e202420204.
(62) Petrželová, K.; Bárta, O.; Héžová, R.; et al. Improved Synthesis of Dinuclear [M(μ-X)(η5-Cp*)X]2 Precursors for Half-Sandwich Complexes (M=Rh or Ir; X=Br or I). *ChemistryOpen* **2025**, *14*, No. e202500026, DOI: 10.1002/open.202500026.
(63) Liu, Z.; Habtemariam, A.; Pizarro, A. M.; et al. Organometallic Half-Sandwich Iridium Anticancer Complexes. *J. Med. Chem.* **2011**, *54*, 3011−3026.
(64) Richter, M. F.; Drown, B. S.; Riley, A. P.; et al. Predictive compound accumulation rules yield a broad-spectrum antibiotic. *Nature* **2017**, *545*, 299−304.
(65) Sievers, R.; Sellin, M.; Rupf, S. M.; Parche, J.; Malischewski, M. Introducing the Perfluorinated Cp* Ligand into Coordination Chemistry. *Angew. Chem., Int. Ed.* **2022**, *61*, No. e202211147.
(66) Nataro, C.; Thomas, L. M.; Angelici, R. J. Cyclopentadienyl Ligand Effects on Enthalpies of Protonation of the Ru−Ru Bond in Cp'2Ru2(CO)4 Complexes. *Inorg. Chem.* **1997**, *36*, 6000−6008.
(67) Johansson, M. P.; Olsen, J. Torsional Barriers and Equilibrium Angle of Biphenyl: Reconciling Theory with Experiment. *J. Chem. Theory Comput.* **2008**, *4*, 1460−1471.
(68) Maher, C.; Hassan, K. A. The Gram-negative permeability barrier: tipping the balance of the in and the out. *mBio* **2023**, *14*, No. e0120523, DOI: 10.1128/mbio.01205-23.
(69) Falanga, A.; Bellavita, R.; Braccia, S.; Galdiero, S. Hydrophobicity: The door to drug delivery. *J. Pept. Sci.* **2024**, *30*, No. e3558.
(70) Kopiasz, R. J.; Zabost, A.; Myszka, M.; et al. Main-chain flexibility and hydrophobicity of ionenes strongly impact their antimicrobial activity: an extended study on drug resistance strains and Mycobacterium. *RSC Adv.* **2022**, *12*, 26220−26232.
(71) Faria, J.; Ahmed, S.; Gerritsen, K. G. F.; Mihaila, S. M.; Masereeuw, R. Kidney-based in vitro models for drug-induced toxicity testing. *Arch. Toxicol.* **2019**, *93*, 3397−3418.
(72) Vaara, M. Agents that increase the permeability of the outer membrane. *Microbiol Rev.* **1992**, *56*, 395−411.
(73) Kim, S. J.; Jo, J.; Kim, J.; Ko, K. S.; Lee, W. Polymyxin B nonapeptide potentiates the eradication of Gram-negative bacterial persisters. *Microbiol. Spectr.* **2024**, *12*, No. e03687-23.
(74) Vaisbourd, E.; Glass, D. S.; Yang, Y.; et al. Principles of bacteriostatic and bactericidal antibiotics at subinhibitory concentrations. *mBio* **2025**, *16*, No. e02066-25.
(75) Liu, Z.; Habtemariam, A.; Pizarro, A. M.; Clarkson, G. J.; Sadler, P. J. Organometallic Iridium(III) Cyclopentadienyl Anticancer Complexes Containing C,N-Chelating Ligands. *Organometallics* **2011**, *30*, 4702−4710.
(76) Schäfer, A.-B.; Sidarta, M.; Nekhala, I. A.; et al. Dissecting antibiotic effects on the cell envelope using bacterial cytological profiling: a phenotypic analysis starter kit. *Microbiol. Spectr.* **2024**, *12*, No. e0327523, DOI: 10.1128/spectrum.03275-23.
(77) Nonejuie, P.; Burkart, M.; Pogliano, K.; Pogliano, J. Bacterial cytological profiling rapidly identifies the cellular pathways targeted by antibacterial molecules. *Proc. Natl. Acad. Sci. U.S.A.* **2013**, *110*, 16169−16174.
(78) Özsan, Ç.; Schäfer, A.; Akhir, A.; et al. A platinum butterfly effect: small changes turn an anticancer drug into a non-toxic metalloantibiotic with in vivo efficacy. *npj Antimicrob. Resist.* **2026**, *4*, No. 37, DOI: 10.1038/s44259-026-00211-w.
(79) te Winkel, J. D.; Gray, D. A.; Seistrup, K. H.; Hamoen, L. W.; Strahl, H. Analysis of Antimicrobial-Triggered Membrane Depolarization Using Voltage Sensitive Dyes. *Front. Cell Dev. Biol.* **2016**, *4*, No. 29, DOI: 10.3389/fcell.2016.00029.
(80) Strahl, H.; Hamoen, L. W. Membrane potential is important for bacterial cell division. *Proc. Natl. Acad. Sci. U.S.A.* **2010**, *107*, 12281−12286.
(81) Kang, H.-J.; Park, H.-J. Novel Molecular Mechanism for Actinomycin D Activity as an Oncogenic Promoter G-Quadruplex Binder. *Biochemistry* **2009**, *48*, 7392−7398.
(82) McCann, M.; McGinley, J.; Ni, K.; et al. A new phenanthroline−oxazine ligand: synthesis, coordination chemistry and atypical DNA binding interaction. *Chem. Commun.* **2013**, *49*, 2341−2343.
(83) Gibney, A.; Sidarta, M.; Delahunt, E.; et al. Expanding the DNA damaging potential of artificial metallo-nucleases with click chemistry. *Nat. Commun.* **2026**, *17*, No. 2309.
(84) Seif, Y.; Monk, J. M.; Mih, N.; et al. A computational knowledge-base elucidates the response of Staphylococcus aureus to different media types. *PLoS Comput. Biol.* **2019**, *15*, No. e1006644.
(85) Smitten, K. L.; Southam, H. M.; de la Serna, J. B.; et al. Using Nanoscopy To Probe the Biological Activity of Antimicrobial Leads

Downloaded from pubs.acs.org/jacsau/article-pdf/doi/10.1021/jacsau.6c00813/6856726/jacsau.6c00813.pdf by UNIV OF YORK user on 06 October 2026

That Display Potent Activity against Pathogenic, Multidrug Resistant, Gram-Negative Bacteria. *ACS Nano* **2019**, *13*, 5133−5146.
(86) Halliwell, B.; Adhikary, A.; Dingfelder, M.; Dizdaroglu, M. Hydroxyl radical is a significant player in oxidative DNA damage in vivo. *Chem. Soc. Rev.* **2021**, *50*, 8355−8360.
(87) Mukherjee, S.; Ghosh, S.; M, R. D.; et al. Peroxiredoxin Depletion and Oxidative Stress by Cyclometalated Ir(III)-Isatin Complexes Renders Ferroptosis and Autophagic Cell Death in Triple-Negative Breast Cancer. *J. Med. Chem.* **2025**, *68*, 21201−21223.
(88) Li, J.; Guo, L.; Tian, Z.; et al. Half-Sandwich Iridium and Ruthenium Complexes: Effective Tracking in Cells and Anticancer Studies. *Inorg. Chem.* **2018**, *57*, 13552−13563.
(89) Cornelis, P.; Wei, Q.; Andrews, S. C.; Vinckx, T. Iron homeostasis and management of oxidative stress response in bacteria. *Metallomics* **2011**, *3*, 540−549.
(90) Ni, W.; Shao, X.; Di, X.; et al. In vitro synergy of polymyxins with other antibiotics for Acinetobacter baumannii: A systematic review and meta-analysis. *Int. J. Antimicrob. Agents* **2015**, *45*, 8−18.

Downloaded from pubs.acs.org/jaaucr/article-pdf/doi/10.1021/jacsau.6c00813/6852726/jacsau.6c00813.pdf by UNIV OF YORK user on 06 October 2026

https://doi.org/10.1021/jacsau.6c00813
JACS Au XXXX, XXX, XXX−XXX